Title

A genome-wide CRISPR screen identifies UFMylation and TRAMP-like complexes as host factors required for hepatitis A virus infection

Journal

Cell Reports, 34(11)

ISSN

2639-1856

Authors

Kulsuptrakul, Jessie
Wang, Ruofan
Meyers, Nathan L
et al.

Publication Date

2021-03-01

DOI

10.1016/j.celrep.2021.108859

Peer reviewed

HHS Public Access

Author manuscript

Cell Rep. Author manuscript; available in PMC 2022 March 16.

Published in final edited form as:

Cell Rep. 2021 March 16; 34(11): 108859. doi:10.1016/j.celrep.2021.108859.

A genome-wide CRISPR screen identifies UFMylation and TRAMP-like complexes as host factors required for hepatitis A virus infection

Jessie Kulsuptrakul[1], **Ruofan Wang**[1], **Nathan L. Meyers**[2], **Melanie Ott**[2,3], **Andreas S. Puschnik**[1,4,*]

[1]Chan Zuckerberg Biohub, San Francisco, CA 94158, USA

[2]Gladstone Institutes, San Francisco, CA 94158, USA

[3]Department of Medicine, University of California, San Francisco, San Francisco, CA 94143, USA

[4]Lead contact

SUMMARY

Hepatitis A virus (HAV) is a positive-sense RNA virus causing acute inflammation of the liver. Here, using a genome-scale CRISPR screen, we provide a comprehensive picture of the cellular factors that are exploited by HAV. We identify genes involved in sialic acid/ganglioside biosynthesis and members of the eukaryotic translation initiation factor complex, corroborating their putative roles for HAV. Additionally, we uncover all components of the cellular machinery for UFMylation, a ubiquitin-like protein modification. We show that HAV translation specifically depends on UFM1 conjugation of the ribosomal protein RPL26. Furthermore, we find that components related to the yeast Trf4/5-Air1/2-Mtr4 polyadenylation (TRAMP) complex are required for viral translation independent of controlling viral poly(A) tails or RNA stability. Finally, we demonstrate that pharmacological inhibition of the TRAMP-like complex decreases HAV replication in hepatocyte cells and human liver organoids, thus providing a strategy for host-directed therapy of HAV infection.

Graphical abstract

*Correspondence: andreas.puschnik@czbiohub.org.

AUTHOR CONTRIBUTIONS

J.K. and A.S.P. were responsible for design and execution of experiments, data analysis, and manuscript preparation. R.W. performed comparative analysis of CRISPR screens and assisted with molecular biology experiments. N.L.M. conducted organoid experiments under the supervision of M.O.A.S.P. conceptualized and supervised the study.

SUPPLEMENTAL INFORMATION

Supplemental Information can be found online at https://doi.org/10.1016/j.celrep.2021.108859.

DECLARATION OF INTERESTS

The authors declare no competing interests.

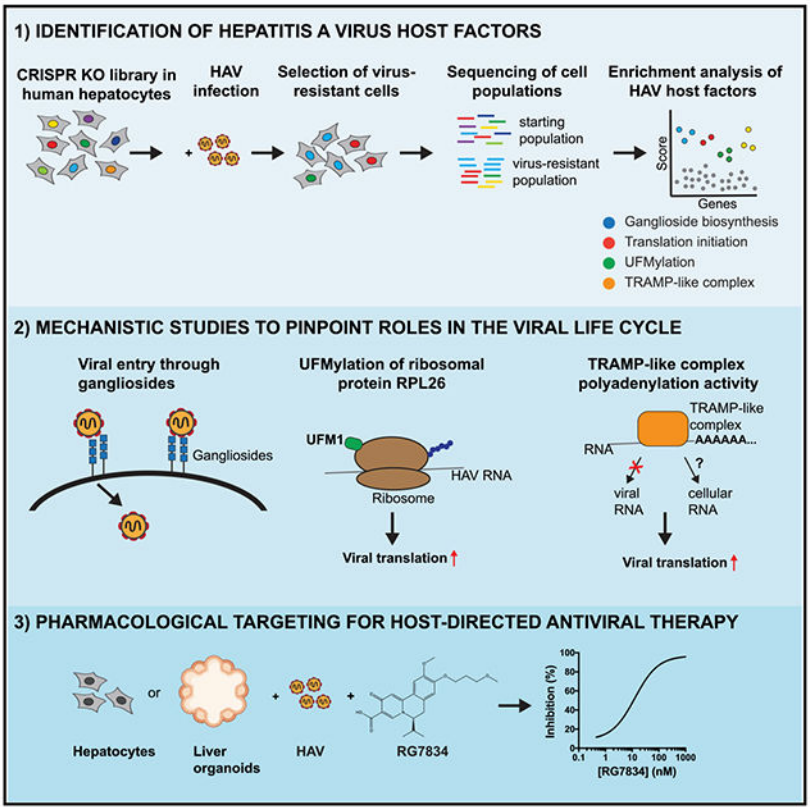

In brief

To identify host factors required for the infection with hepatitis A virus, Kulsuptrakul et al. conducted a genome-wide CRISPR knockout screen in human hepatocytes. They reveal that UFMylation of the ribosomal protein RPL26 as well as the polyadenylation activity of a TRAMP-like complex enhance viral translation.

INTRODUCTION

Hepatitis A virus (HAV) is a single-stranded, positive-sense RNA virus and a hepatotropic member of the *Picornaviridae*. Despite successes in vaccine development, HAV remains a common cause of enterically transmitted hepatitis globally, responsible for epidemics in developing and developed countries, and with symptoms ranging from mild inflammation and jaundice to acute liver failure (CDC, 2019; Jacobsen, 2018). However, no specific antiviral treatment is currently available. Thus, a better understanding of the molecular virus-host interactions is important and can provide insights for host-directed therapies.

During infection, HAV enters host cells through interaction with sialic acid and ganglioside molecules, followed by uncoating and delivery of viral RNA from endosomes to the cytosol (Das et al., 2020). The genomic RNA is translated into a polyprotein and subsequently processed into the individual structural and non-structural proteins. HAV then co-opts cellular membranes to form virus-specific organelles, where genome replication occurs

(McKnight and Lemon, 2018). Finally, the newly synthesized genomes are packaged, and HAV egresses in the form of quasi-enveloped virions (Feng et al., 2014).

Despite a general understanding of the viral life cycle and suggested roles for certain cellular proteins during infection, a comprehensive assessment and thorough validation of the most critical host factors for HAV infection is lacking. For example, TIM1 (T cell immunoglobulin mucin receptor 1), also named HAV cellular receptor 1 (HAVCR1), was originally identified as receptor for HAV, but a more recent study disproved its essentiality for HAV infection (Das et al., 2017; Kaplan et al., 1996).

Additionally, numerous host proteins have been shown to interact with the viral RNA to potentially modulate translation or replication of the HAV genome. For example, the HAV internal ribosome binding site (IRES) is unique in that it requires an intact cellular eukaryotic translation initiation factor complex, while other picornaviruses shut down host mRNA translation by proteolytic cleavage (Ali et al., 2001; Borman and Kean, 1997). Other RNA binding proteins, such as PCBP2 (Poly(RC) binding protein 2), PTBP1 (Polypyrimidine tract-binding protein 1)n or La protein have been shown to bind viral RNA, but their importance in viral translation or replication are not fully determined (Gosert et al., 2000; Graff et al., 1998; Jiang et al., 2014).

To address these knowledge gaps, we performed a genome-wide CRISPR knockout (KO) screen to identify host cellular factors that are critical for the HAV life cycle in an unbiased fashion. CRISPR screens have successfully been used to study human pathogens, such as mosquito-borne flaviviruses, enteroviruses, or hepatitis C virus (HCV) (Diep et al., 2019; Marceau et al., 2016; Zhang et al., 2016).

Using this approach, we identified sialic acid and ganglioside biosynthesis genes, important for viral entry, as well as factors of the eukaryotic translation initiation factor complex and PTBP1, previously implicated in HAV translation. Additionally, we uncovered unknown cellular pathways, in particular, UFMylation and a TRAMP-like complex (related to the yeast Trf4/5-Air1/2-Mtr4 polyadenylation complex) and pinpoint their role to HAV protein synthesis. Importantly, we demonstrated that these host factor requirements are largely unique to HAV compared to other picornaviruses. Surprisingly, a comparison with host factors for hepatitis B virus (HBV), a DNA virus with a vastly different replication strategy, revealed a shared dependency on the TRAMP-like complex protein ZCCHC14, thus highlighting an unexpected convergence across different viral families to co-opt the same cellular complex (Hyrina et al., 2019). Finally, we provided proof-of-concept data for host-directed therapy of HAV infections using a small-molecule inhibitor against subunits of the TRAMP-like complex.

RESULTS

A genome-wide CRISPR screen reveals host factors required for HAV infection

To identify host cellular factors that are critical for HAV infection, we conducted a genome-wide CRISPR KO screen in the human hepatocyte cell line Huh7.5.1 using the cytopathic HAV HM175/18f strain (Lemon et al., 1991; Figure 1A). Infection led to approximately

90% cell death by day 5; the remaining cells were re-infected at day 7, and surviving cells were collected after 12 days for analysis. We found enrichment of guide RNA (gRNA) sequences targeting genes involved in several pathways known to be required for HAV replication (Figure 1B; Table S1). For example, sialic acid and ganglioside biosynthesis genes (*GNE, CMAS, SLC35A1, UGCG, ST3GAL5*) were recently described to express endosomal receptors for HAV and other viruses (Baggen et al., 2016; Das et al., 2020; Ding et al., 2018; Drake et al., 2017; Han et al., 2018). We also identified *PTBP1* and members of the eukaryotic translation initiation factor complex (*EIF4B, EIF3C, EIF3CL*), which have known roles in IRES-mediated translation of HAV and other picornaviruses (Avanzino et al., 2017; Borman and Kean, 1997; Gosert et al., 2000; Pestova et al., 1996). The highly enriched VPS4Ais an AAA-ATPase that regulates endosomal sorting complexes required for transport (ESCRT) and has been implicated in budding of several enveloped viruses as well as egress of HAV (Feng et al., 2013; Votteler and Sundquist, 2013). Together, the identification of host components previously linked to HAV infection validates the phenotypic selection in our CRISPR screen.

Importantly, gene ontology (GO) analysis of enriched genes (RIGER $p < 0.001$) revealed additional pathways that have not previously been linked to HAV infection (Figure 1C; Tables S1 and S2). First, we identified several known components of the machinery for UFMylation (*UFM1, UBA5, UFL1, UFC1, UFSP2*), a ubiquitin-like protein modification (Gerakis et al., 2019; Komatsu et al., 2004; Figures 1B and 1C). Second, the two related non-canonical poly(A) RNA polymerases, PAPD5 (also known as TENT4B or TRF4-2) and PAPD7 (also known as TENT4A or TRF4-1) were notably enriched (Figures 1B and 1C; Warkocki et al., 2018). Finally, ZCCHC14 (Zinc Finger CCHC Domain-Containing Protein 14), the second most enriched gene, has been shown to associate with PAPD5 and PAPD7, and act as a cofactor for RNA binding (Figure 1B; Hyrina et al., 2019; Kim et al., 2020). Together, these proteins form a so-called TRAMP-like complex, which generally contain a RNA polymerase and zinc finger protein (Hamill et al., 2010; Lubas et al., 2011).

To assess the specificity of the identified cell components across different viral infections, we systematically compared our hits with CRISPR screens for host factors of human rhinovirus C15 (HRV-C15) and enterovirus D68 (EV-D68), two distantly related picornaviruses (Diep et al., 2019). Despite differences in tissue tropism and pathogenesis, HAV shares common replication strategies with other members of the *Picornaviridae* family to translate and synthesize its genomes. However, other than sialic acid biosynthesis genes among the EV-D68 hits, there were no commonalities among the most crucial identified host factors in these screens, indicating divergent evolution of host factor dependencies (Figures S1A and S1B). Next, we compared our results to a CRISPR screen for HCV infection, another hepatotropic positive-sense RNA virus (and member of the *Flaviviridae* family) but found no overlap in the host factor requirements (Figure S1C; Marceau et al., 2016).

Last, a comparison with results from a CRISPR screen for hepatitis B virus (HBV), a DNA virus replicating through reverse transcription, highlighted ZCCHC14 as a shared host dependency factor between HAV and HBV (Figure S1D; Hyrina et al., 2019). Together, these data illustrate that the host factor requirements for HAV are largely unique compared

to other picornaviruses but reveal an unexpected commonality between HAV and HBV infection.

Knockout of identified host factor genes impairs HAV replication

To validate the results of our screen, we generated isogenic Huh7.5.1 KO cell lines in several genes by CRISPR-Cas9 gene editing, which resulted in frameshifts and loss of protein expression (Figures S2A–S2C). Upon HAV infection, we observed significant reduction of both viral replication and virion production ranging from 10 to 1,000-fold relative to levels in wild-type (WT) cells at 72 h post-infection (hpi) (Figures 2A and S3A). As PAPD5 and PAPD7 are both human orthologs of yeast Trf4p and display partial redundancy in their polyadenylation function (Warkocki et al., 2018), we generated *PAPD5/PAPD7* double-knockout (DKO) cell lines (Figure S2A). We observed a significantly stronger reduction in viral replication in the DKO cells compared to the single *PAPD5* or *PAPD7* KO cells underscoring their redundant activity for HAV replication (Figure 2B). To assess viral growth phenotypes over time, we performed an infection assay using a recombinant reporter virus that expresses nanoluciferase from within its polyprotein (HAV-NLuc). We measured an ~10^4-fold increase in luminescence in WT cells after 72 hpi, but there was striking attenuation of luciferase expression in host factor KO lines, highlighting that the growth defect persists through multiple replication cycles (Figure 2C). Importantly, when we complemented *UBA5, PAPD5,* and *ZCCHC14* KO cells with the respective cDNAs, we observed a significant increase in HAV replication (Figures 2D–2F and S2C).

It is of note that our screen did not reveal HAVCR1 (TIM1) as an essential host factor for HAV infection. To address this further, we performed a viral attachment and internalization assay in isogenic *HAVCR1* KO cells (Figure S2A). We only observed a minor defect of internalized viral RNA at 6 hpi and viral RNA levels were only reduced by 2-fold relative to WT cells at 30 hpi (Figure S3B). By contrast, in *SLC35A1* KO cells intracellular viral RNA was decreased 5-fold at 6 hpi and >20-fold at 30 hpi. We conclude that *HAVCR1* is not absolutely critical for the HAV life cycle, while sialic acid biosynthesis is important for efficient viral entry. Overall, the genetic KO studies confirm that the CRISPR screen identified genes with robust roles in the HAV life cycle.

Finally, we confirmed the finding from the comparative CRISPR screen analysis that the newly implicated UFMylation machinery and TRAMP-like complexes are distinct to HAV among different *Picornaviridae* members. HAV RNA levels were greatly reduced while enterovirus 71 (EV-71) and encephalomyocarditis virus (EMCV) RNA levels were not affected in *UFM1* KO cells (Figure 2G). Interestingly, human rhinovirus A2 (RV-A2) replication was increased suggesting that UFMylation can mediate pro- and antiviral functions in host cells depending on the virus species. Similarly, in cells deficient in both PAPD5 and PAPD7, HAV RNA levels were severely and EMCV RNA levels moderately decreased while EV-71 and RV-A2 replication were unaffected (Figure 2H). Together, these data confirm that UFMylation and TRAMP-like complex components have important and largely distinct functions in the HAV life cycle but not for other picornaviruses.

HAV depends on UFMylation of the ribosomal protein RPL26 for efficient translation

Struck by the unique dependency of HAV on UFMylation and no described role in viral infection, we first followed up on this cellular pathway. *UFM1* encodes the 85 amino acid long ubiquitin-fold modifier 1, which acts as a protein modification and is conserved among most eukaryotes except for yeast and other fungi (Komatsu et al., 2004). Like ubiquitination, UFM1 is covalently attached to its targets following an E1-E2-E3 reaction consisting of the UFM1-activating enzyme UBA5, the UFM1-conjugating enzyme UFC1, and the UFM1-specific ligase UFL1 (Figure 3A; Komatsu et al., 2004; Tatsumi et al., 2010). Usually, UFM1 is present in a precursor form, which first requires cleavage of the last two C-terminal amino acids by UFM1-specific proteases UFSP1 or UFSP2 to expose the glycine at position 83 (Kang et al., 2007). UFSP2 also operates as the major de-UFMylation enzyme, removing UFM1 molecules from their targets (Ha et al., 2011; Kang et al., 2007). Our screen identified all known components of the UFMylation machinery including the additionally associated proteins DDRGK1 and ODR4 (encoded by *C1orf27*) (Figure 3A; Chen et al., 2014; Wu et al., 2010). WT cells contain free UFM1 as well as conjugated UFM1 as detected by immunoblot (Figure 3B). To probe whether functional conjugation of UFM1 is required for HAV infection, we mutated different components of the pathway. Deletion of *UBA5* led to an absence of conjugated UFM1 while *UFSP2* KO resulted in hyper-conjugation consistent with their reported activities (Figure 3B). Both conditions led to a stark reduction of viral RNA in infected cells, suggesting that the modification needs to be reversible for its proviral function (Figure 3C). Moreover, we reconstituted *UFM1* KO cells with WT-UFM1, a more stable UFM1(Gly83Ala) modification or UFM1(ΔC3), which lacks the last 3 C-terminal amino acids essential for conjugation (Figure 3B; Komatsu et al., 2004). Complementation with WT-UFM1 and UFM1(Gly83Ala) significantly restored HAV replication (Figure 3C). By contrast, conjugation-deficient UFM1(ΔC3) did not rescue viral infection. Consistent with this, complementation of *UBA5* KO cells with WT-UBA5 but not catalytically inactive enzyme (UBA5(cat)) also restored UFM1 conjugation and viral replication (Figures 3B, S2C, and S4A). Together, these data establish that functional and reversible UFM1 conjugation is critical for HAV replication.

Next, in order to assess whether the defect occurs during early viral translation or later during the genome replication step, we used HAV replicon RNA expressing firefly luciferase (Fluc). We detected a marked defect of Fluc expression in *UBA5, UFSP2*, and *UFM1* KO cells within 10 h post-electroporation, which increased further post-24 h relative to WT cells (Figures 3D and S4B). To exclusively measure the effect on translation of incoming viral RNA, we used a replication-incompetent replicon (containing a GDD→GAA mutation in the viral polymerase) and observed strongly reduced Fluc expression in all KO cells (Figures 3E and S4C). We excluded that observed phenotypes were due to drastic differences in cell viability or proliferation post-electroporation (Figure S4D). We therefore conclude that UFMylation is required for optimal translation of HAV RNA.

Recently, the ribosomal protein RPL26 was identified as a major target for UFMylation in human cells (Walczak et al., 2019; Wang et al., 2020). Thus, we tested whether UFMylated RPL26 is important for efficient HAV translation. Consistent with previous findings, we detected modified RPL26 at the molecular weight corresponding to UFM1 conjugates

(Figure 3F). Interestingly, only a small fraction of RPL26 is UFMylated and the conjugation appears transient as it can only be visualized in *UFSP2* KO cells, which lack de-UFMylase activity. It was further shown that conjugation of UFM1 occurs at C-terminal lysines of RPL26 (Walczak et al., 2019; Wang et al., 2020). We generated cell lines with ectopic WT-RPL26 or RPL26 containing five lysine to arginine substitutions (5KR-RPL26) and showed that only WT- but not 5KR-RPL26 was UFMylated (Figures 3G and S4E). We additionally confirmed specific UFM1 conjugation of WT-RPL26 by immunoprecipitation (Figure S4F). HAV infection of WT Huh7.5.1 cells expressing 5KR-RPL26 was reduced compared to cells containing ectopic WT-RPL26, which largely phenocopied the *UFM1* KO effect (Figure 3H). By contrast, there was no dominant-negative effect of 5KR-RPL26 in transduced *UFM1* or *UFSP2* KO cells; deletion of *UFM1* or *UFSP2* already reduced replication to levels similar to WT Huh7.5.1 containing 5KR-RPL26 (Figure 3H). We also measured reduced HAV replication in previously characterized U2OS cells expressing 5KR-RPL26 and a CRISPRi system to knock down endogenous WT-RPL26 (Walczak et al., 2019; Figure S4G). Last, 5KR-RPL26 cells exhibited increased RV-A2 infection (Figure S4H), thus mirroring the effect of *UFM1* deletion (Figure 2G). Together, the results indicate that UFM1 and RPL26 are functionally linked and support a model where HAV requires active UFMylation of RPL26 for translation.

TRAMP-like complexes support HAV translation independent of polyadenylation of HAV tails or stabilization of viral RNA

Intrigued by the strong phenotypes on HAV replication and a critical role in the life cycles of both HAV and HBV, we performed mechanistic studies on the TRAMP-like complex components PAPD5, PAPD7, and ZCCHC14. The two non-canonical poly(A) RNA polymerases PAPD5 and PAPD7 can transfer poly or oligo(A) to a variety of RNA substrates (e.g., mRNAs, miRNAs, snoRNAs, and rRNAs) in a template-independent manner (Berndt et al., 2012; Boele et al., 2014; Rammelt et al., 2011; Shcherbik et al., 2010; Shin et al., 2017). Their cellular activities include stabilization of mRNAs for translation as well as specifying different RNA species for turnover by the exosome complex (Lubas et al., 2011; Vanácová et al., 2005; Warkocki et al., 2018). Recently, ZCCHC14 has been shown to interact with PAPD5 and PAPD7 to bind and stabilize HBV RNAs (Hyrina et al., 2019; Kim et al., 2020); consistent with this, we observed strong reduction of HBV RNA levels in *ZCCHC14* KO cells (Figure S5A).

To determine the function of the TRAMP-like complex during HAV infection, we first measured the effects of *PAPD5/7* DKO or *ZCCHC14* KO on viral translation and replication using viral replicon RNA. We observed a notable defect in luciferase expression immediately post-electroporation, suggesting inefficient translation of viral RNA (Figure 4A). While WT cells supported replicon replication at later time points, luminescence decayed to background levels in the KO cells. Northern blot confirmed absence of any detectable HAV RNA in the KO cells at 72 hpi (Figure S5B). We additionally probed viral translation directly using the replication-incompetent HAV replicon and observed drastically reduced luciferase expression from incoming RNA immediately post-electroporation in DKO and *ZCCHC14* KO cells (Figure 4B). By contrast, translation of electroporated Fluc mRNA was not affected, excluding a general translation defect in KO cells (Figure S5C).

As translation from viral RNA is directly linked to RNA stability, we measured decay of electroporated replication-deficient HAV replicon in WT and DKO cells by northern blot, but we did not observe notable differences (Figure 4C). We therefore conclude that deletion of TRAMP-complex components affects HAV translation independent of general HAV genome stability.

For HBV, mechanistic studies revealed that HBV surface antigen expression requires mixed tailing of HBV mRNAs by TRAMP-like complexes (Kim et al., 2020). This low-frequency introduction of mostly guanosines into poly(A) tails can result in increased stability against CCR4-NOT-dependent deadenylation (Lim et al., 2018). As HAV has a polyadenylated genome and longer poly(A) tails can promote translation (Bergamini et al., 2000; Chen et al., 2018), we assessed the length distribution of HAV poly(A) tails from infected WT, DKO, and *ZCCHC14* KO cells by polyacrylamide gel electrophoresis. However, we did not observe a notable difference (Figure 4D). By contrast, HBV tails were reduced in *ZCCHC14* KO cells, confirming the expected phenotype (Figure 4D). We additionally performed TOPO cloning followed by Sanger sequencing as well as a high-resolution electrophoretic shift assay using TapeStation, confirming that HAV tails were not shortened in KO cells (Figures 4E and S5D). Finally, we corroborated the results with an oligo(dT)/RNase H-northern blot analysis, which does not rely on PCR amplification of the poly(A) tail region (Sallés et al., 1999). We detected a band shift for HAV RNA upon oligo(dT)/RNase H treatment isolated from both WT as well as DKO cells (Figure S5E), indicating that HAV tails have comparable lengths. Therefore, the different methods for poly(A) tail length determination are in agreement that the TRAMP-like complex is not responsible for HAV polyadenylation.

As PAPD5 and PAPD7 can introduce guanosines at low frequencies into poly(A) tails, we analyzed the nucleotide composition of the HAV poly(A) tails from RNA isolated from WT or DKO cells. We did not observe an elevated frequency of non-adenosine nucleotides in WT relative to DKO cells within HAV poly(A) tails (Figure 4F). Rather, almost all analyzed tails exclusively consisted of adenosines in both conditions. Together, our data suggest that TRAMP-like complexes do not modulate the length or composition of HAV poly(A) tails.

As the described cellular functions of PAPD5 and PAPD7 depend on their catalytic activity, we complemented KO or DKO cells with WT or catalytically inactive (cat) PAPD5 and/or PAPD7 cDNAs, which contain two aspartate to alanine substitutions in the active site (Figure S2C; Rammelt et al., 2011). Infection of the complemented cell lines established that the catalytic activities of PAPD5 and PAPD7 are required to support viral replication (Figures 4G and S5F). In conclusion, we find that the catalytic activity is required to support viral translation, independent of direct modulation of viral poly(A) tails and RNA stability.

Pharmacological inhibition of PAPD5 and PAPD7 exhibits an antiviral effect against HAV infection

As the enzymatic function of PAPD5 and PAPD7 are required for HAV infection, we explored whether pharmacological inhibition has an antiviral effect. We used RG7834 (Figure 5A), a small-molecule compound belonging to the chemical class of the dihydroquinolizinones. This compound was first identified as a potent inhibitor for HBV

surface antigen secretion (Mueller et al., 2018), and PAPD5 and PAPD7 were subsequently shown to be its cellular targets (Mueller et al., 2019).

To test whether RG7834 also exhibits activity against HAV replication, we performed a dose-response curve and calculated a 50% effective concentration (EC_{50}) of 12.76 nM for inhibition of HAV replication (Figure 5B). This is far below the measured 50% cytotoxic concentration (CC_{50}) of >10 μM (Figure S5G). Drug treatment of infected *PAPD5* or *PAPD7* KO cells suggested that RG7834 has a stronger inhibitory effect on the PAPD5 activity as reduction of viral RNA was more substantial in the *PAPD7* KO+RG7834 condition (Figure S5H). Intrigued by the fact that RG7834 inhibits both HAV and HBV, we also measured the effects on two additional liver-specific viruses, HCV and hepatitis E virus (HEV). However, RG7834 only showed significant reduction of HAV and HBV RNA levels (Figures 5C–5F). This is consistent with the comparative CRISPR screen analysis for HCV as well as unchanged viral replication levels in DKO cells for both HCV and HEV (Figure S5I).

Finally, we performed infection assays in human liver organoid cultures (Broutier et al., 2016). We observed significant dose-dependent reduction of HAV RNA in both stem cell-like and differentiated organoids under RG7834 treatment (Figures 5G and S5J). Together, our results demonstrate that pharmacological inhibition of PAPD5/7 is a promising strategy for host-directed therapy of HAV infection.

DISCUSSION

This study provides a comprehensive assessment of the host factors that are critical for HAV infection. The identified genes comprise several cellular pathways and complexes, such as sialic acid biosynthesis, eukaryotic translation initiation, UFMylation, TRAMP-like complexes, and others. We corroborated that the putative HAV receptor, HAVCR1, is not essential for infection. Rather, we found multiple genes linked to sialic acid and ganglioside biosynthesis, which are important for efficient HAV uptake (Das et al., 2020). The screen also identified eukaryotic translation initiation factor components and PTBP1, which were previously linked to HAV translation (Avanzino et al., 2017; Borman and Kean, 1997; Gosert et al., 2000; Pestova et al., 1996).

Importantly, we revealed two cellular pathways, UFMylation and TRAMP-like complexes, which had not been implicated in HAV life cycle before. UFMylation is a ubiquitin-like, post-translation modification. The cellular function of this protein modification is still an emerging field of research, but it has been linked to the regulation of the ER stress response, ribosome-associated quality control, and ER phagy (Liang et al., 2020; Walczak et al., 2019; Wang et al., 2020). The ribosomal protein RPL26 has been identified as a major target for UFMylation (Walczak et al., 2019; Wang et al., 2020). We demonstrated that HAV specifically depends on UFMylation of RPL26 for efficient translation. Specific ribosomal or ribosome-associated proteins have been shown to be required for efficient translation of other viral genomes (Jha et al., 2017; Landry et al.,2009; Majzoub et al.,2014). RPL26 is located near the ribosome exit tunnel and its modification could facilitate dynamic and reversible conformation changes to improve translation of specific amino acid sequences

or resolve certain secondary structure in the RNA as suggested by the requirement for active UFMylation and de-UFMylation during HAV infection. Additional studies, such as biochemical analysis and ribosome profiling of the different ribosomal subpopulations, are needed to gain a better understanding of its role during translation of viral and cellular mRNAs. The contrasting phenotypes observed during HAV and RV-A2 infection in *UFM1* KO cells may be utilized as tools for future studies of the molecular effects of UFMylation.

Furthermore, we identified the TRAMP-like complex components ZCCHC14, PAPD5, and PAPD7 and demonstrated that they are required for HAV translation. PAPD5 and PAPD7 have been described to possess polyadenylation activity as well as the ability to generate mixed tails, which can increase RNA stability (Lim et al., 2018; Warkocki et al., 2018). Despite showing that their catalytic activities are required to support HAV infection, we did not observe any abnormalities in HAV poly(A) tail length, poly(A) tail nucleotide composition, or overall viral RNA stability in TRAMP-like complex-deficient cells. However, this is consistent with previous observations that picornavirus polyadenylation is template dependent, for example, by the presence of a homotypic poly(U) sequence in the picornavirus negative-sense RNA (Spector and Baltimore, 1975). Moreover, studies using poliovirus, another picornavirus, suggested that the picornaviral RNA-dependent RNA polymerase uses reiterative transcription as it replicates the poly(A) tails of viral RNA (Kempf et al., 2013; Steil et al., 2010). These findings support that PAPD5 and PAPD7 are not necessarily required for HAV poly(A) tail generation or maintenance. We therefore hypothesize that the TRAMP-like complexes either directly modulate HAV RNA in a so-far-unrecognized manner or that expression of a cellular protein, which is critical for HAV translation, depends on polyadenylation of its mRNA. In studies using *C. elegans*, deletion of the worm orthologs of PAPD5 (gld-4) and ZCCHC14 (gls-1) led to reduced polysome formation but did not affect global poly(A) tail lengths, providing evidence of polyadenylation-independent functions of TRAMP-like complexes (Nousch et al., 2014).

For HBV, it has been shown that ZCCHC14 directly interacts with a CNGGN-type pentaloop in the viral mRNAs to generate mixed tails, protect viral poly(A) tails from deadenylation, and ultimately increase mRNA stability for surface antigen expression (Hyrina et al., 2019; Kim et al., 2020; Mueller et al., 2019). This is in contrast with the role of the TRAMP-like complex for HAV, where we did not observe any effects on HAV RNA. It therefore will be interesting to test whether HAV RNA or rather cellular mRNAs are bound to ZCCHC14 through a similar motif. Overall, this highlights a remarkable convergence of two unrelated hepatitis viruses to co-opt the same cellular complex in different ways.

Finally, based on the identification of the TRAMP-like complex as critical HAV host factor we provided proof of concept that pharmacological inhibition of PAPD5 and PAPD7 decreases infection levels and may thus be pursued for the treatment of severe HAV infections. In summary, this study exemplifies that host factor screens are a powerful strategy to gain a comprehensive understanding of the most critical cellular pathways for viral infections, and to illuminate new drug targets, which can be shared across different viral families.

STAR★METHODS

RESOURCE AVAILABILITY

Lead contact—Further information and requests for resources and reagents should be directed to and will be fulfilled by the Lead Contact, Andreas S. Puschnik (andreas.puschnik@czbiohub.org).

Materials availability—All requests for resources and reagents should be directed to and will be fulfilled by the Lead Contact author. Materials will be made available through the authors upon execution of a Material Transfer Agreement.

Data and code availability—The accession number for the raw sequencing data of the CRISPR KO screens reported in this paper is EMBL-EBI ArrayExpress: E-MTAB-8646

EXPERIMENTAL MODEL AND SUBJECT DETAILS

Cell lines, viruses, and reagents—Huh7.5.1 (gift from Frank Chisari) (Zhong et al., 2005), HEK293FT (Thermo Scientific) and U2OS cells (gift from Ron Kopito) (Walczak et al., 2019) were cultured in DMEM (GIBCO) supplemented with 10% fetal bovine serum (FBS, Omega Scientific), penicillin/streptomycin (GIBCO), non-essential amino acids (GIBCO) and L-glutamine (GIBCO) at 37C and 5% CO_2. HepG2-NTCP-K7 cells (gift from Ulrike Protzer) (Ko et al., 2018) and HepAD38 cells (gift from Christoph Seeger) (Ladner et al., 1997) were cultured in DMEM/F12 (GIBCO) supplemented with 10% FBS, penicillin/streptomycin, non-essential amino acids, L-glutamine and sodium pyruvate (GIBCO) at 37C and 5% CO_2. All cell lines were tested negative for mycoplasma. Huh7.5.1 were authenticated by STR profiling. Hepatitis A virus HM175/18f (NR-137) was obtained through BEI Resources (NIAID, NIH) and propagated in Huh7.5.1 cells grown in adeno expression media (GIBCO) supplemented with penicillin/streptomycin, non-essential amino acids and L-glutamine. Supernatant was collected 5-12 dpi and filtered (0.45 micron). To generate concentrated HAV stocks, supernatant was incubated with 8% PEG-8000 at 4C overnight, centrifuged at 3,200 g for 60min and pellet was resuspended in a small volume of DMEM with 10% FBS and aliquoted. HAV stocks were titered in a focus-forming assay by performing a 10-fold dilution series and immunofluorescence staining against dsRNA and viral antigen (VP3). For the generation of HAV-Nluc (gift from Stanley Lemon) (Rivera-Serrano et al., 2019), the infectious clone plasmid was linearized, RNA was *in-vitro* transcribed using MEGAscript T7 Transcription Kit (Invitrogen) and transfected into Huh7.5.1 cells using TransIT-LT1 Transfection Reagent (Mirus Bio). Subsequently, cell supernatant was collected 8-13dpi, filtered and aliquoted. Purified encephalomyocarditis virus (NR-46441) was obtained through BEI Resources (NIAID, NIH). Enterovirus 71 (MP4 strain) (Huang et al., 2012), rhinovirus A2 (ATCC, VR-482) and HCV JFH1 (Wakita et al., 2005) stocks were kindly provided by Jan Carette. For HBV production, supernatant was collected from HepAD38 cells, filtered (0.45 micron), and concentrated using 8% PEG-8000 as described above. The HEV infectious clone (genotype 3) was obtained from the NIH/NIAID and viral RNA was generated by *in-vitro* transcription from linearized plasmid (Shukla et al., 2012). RG7834 was purchased from MedKoo Biosciences and resuspended in DMSO at 50mg/ml. Puromycin and blasticidin were obtained from GIBCO.

METHOD DETAILS

CRISPR host factor screen—Huh7.5.1 cells were stably transduced with lentivirus from lentiCas9-Blast (Addgene #52962, gift from Feng Zhang) (Sanjana et al., 2014) and subsequently selected using blasticidin. Next, a total of 300 million Huh7.5.1-Cas9 cells were then separately transduced with the lentiviral gRNA sublibraries A and B of the human GeCKO v2 library (Addgene #1000000049, gift from Feng Zhang) (Sanjana et al., 2014) at a multiplicity of infection (MOI) of 0.3. Each sublibrary contained 3 guides per gene. Subsequently, the cells were selected using puromycin and expanded for 10 days. A total of 60 million mutagenized cells for each sublibrary (A and B) were collected for genomic DNA (gDNA) extraction of the starting population, and a total of 45 million mutagenized cells from each sublibrary were infected with HAV HM175/18f at a MOI of 10 in T175 flasks in a total volume of 15ml per flask. An additional 15ml of media was added after 2h. Media was refreshed at day 4 and cells were re-infected with a MOI~10 at 7 dpi. Additional virus replication and spread likely led to multiple rounds of infection in each cell. Surviving cells continued to divide and approximately 55 million cells per sublibrary were collected 12 dpi for gDNA extraction using QIAamp DNA Blood Maxi Kit (QIAGEN). The HAV CRISPR screen was performed once.

gRNA encoding DNA sequences were amplified in a two-step nested PCR using KAPA HiFi HotStart ReadyMixPCR Kit (Kapa Biosystems). For PCR1, 40 reactions containing 8 μg gDNA were set up and amplified for 16 cycles. Reactions for each sample were pooled and mixed. For PCR2, 4 reactions containing 5 μL PCR1 product were amplified for 12 cycles using indexed primers. PCR products were gel purified using QIAquick Gel Extraction Kit (QIAGEN) and sequenced on an Illumina NextSeq 500 using a custom sequencing primer. Primers sequences are listed in Table S3.

For analysis, demultiplexed FASTQ files were aligned to gRNA reference table and enrichment of each gRNA was calculated by comparing the relative abundance in the selected and unselected cell population. Gene enrichment analysis was performed using the RIGER weighted sum algorithm as well as MaGeCK analysis (Li et al., 2014; Luo et al., 2008). Gene ontology analysis of enriched genes in target list (containing 72 genes with RIGER p value < 0.001) was performed using GOrilla (Eden et al., 2009). For comparison with other CRISPR host factor screens, RIGER-based gene enrichment analysis was used for HCV and HBV screens, and MaGeCK-based analysis for EV-D68 and HRV-C15 screens.

Generation of clonal KO cell lines—DNA oligos (Integrated DNA Technologies) containing gRNA sequences were annealed and ligated into pX458 (Addgene #48138, gift from Feng Zhang) (Ran et al., 2013). Cells were transfected with pX458 constructs using Lipofectamine 3000 (Invitrogen) and two days later GFP-positive cells were single-cell sorted into 96-well plates using a Sony SH800 cell sorter. For genotyping, gDNA was isolated from obtained clones using QuickExtract (Lucigen), the gRNA-targeted sites were PCR-amplified and the products Sanger-sequenced. Reads were aligned to reference sequences and analyzed for presence of indel mutations or large deletions using Geneious Prime (Geneious). Double traces from heterozygous clones were deconvoluted using ICE

analysis (https://ice.synthego.com/#/) (Hsiau et al., 2019). A list of all used gRNA oligo and genotyping primer sequences can be found in Table S3.

Intracellular RNA qRT-PCR assays—Cells were plated in 96-well plates (in 3 biological replicates for each condition) and infected the next day with virus at the following MOIs: HAV (~5-10 focus forming units/cell), RV-A2 (~1 plaque forming units/cell), EV-71 (~0.2 plaque forming units/cell), EMCV (~0.2 plaque forming units/cell), HCV (~1 focus forming units/cell) and HBV (~1 focus forming units/cell). Cells were harvested, lysates reverse transcribed and quantitative PCR performed on a Bio-Rad CFX96 Touch system using the Power SYBR Cells-to-CT kit (Invitrogen). All viral RNA levels were normalized to 18S levels. Primer sequences can be found in Table S3.

Quantification of extracellular viral RNA—Cells were plated in 96-well plates (duplicates for each condition) and infected with HAV at an MOI of 5. After 4h, inoculum was removed and cells were washed with PBS. At 3 dpi 100 µL of supernatant was collected and RNA was isolated using the QIAGEN Viral RNA Mini kit. Eluted RNA was reversed transcribed and analyzed by qPCR as described above. For determination of genome copies, *in-vitro* transcribed HAV RNA was serially diluted and also quantified by qRT-PCR.

Viral attachment and entry assay—96-well plates containing WT, *SLC35A1* KO or *HAVCR1* KO Huh7.5.1 cells were chilled on ice before infection with HAV HM175/18f at an MOI of 500 focus forming units/cell. Cells were incubated for 1h on ice before moving them to a 37C incubator. At each harvest time point, cells were washed three times with PBS and processed for qRT-PCR as described above.

HAV nanoluciferase reporter assay—Cells were plated in 96-well plates and infected the next day with equal amounts of HAV-Nluc. Lysates were harvested by washing once with PBS wash followed by addition of 22 µl of Passive Lysis Buffer (Promega) under shaking for 15 min. For luminescence readout, 15 µl of lysate were mixed with 50 µl of Nano-Glo assay buffer (Promega) in a flat bottom white-walled luminescence plate, incubated for 5 min at room temperature and read on an EnVision plate reader (PerkinElmer).

Complementation of KO cells with cDNA—UBA5 cDNA was obtained from Dharmacon (DNA Accession: BC009737, Clone ID: 3879061). To generate cDNA encoding catalytically inactive enzyme, a Cys250Arg mutation was introduced by PCR. Additionally, a C-terminal FLAG-tag was added to WT and cat cDNA sequences. UFM1 was obtained from Dharmacon (cDNA Accession: BC005193, Clone ID: 3829206). N-terminal FLAG and C-terminal mutations (Gly83Ala or ΔC3 (deletion of GlySerCys)) were introduced by PCR. For RPL26, cDNA was obtained from OriGene (RC209922) and a C-terminal FLAG-tag was added. To introduce 5KR mutations, a reverse primer containing 5 point mutations was used. ZCCHC14 cDNA was obtained from Dharmacon (cDNA Accession: BC101478, Clone ID: 8068984). The N terminus was extended using a gblock (Integrated DNA Technologies) resembling the protein coding sequence for a longer isoform (1086 amino acids, ENST00000671377.1) to match the molecular weight of ZCCHC14 detected in WT Huh7.5.1 by immunoblot. PCR products were gel-purified and cloned into EcoRV-cut pLenti

CMV Puro DEST (w118-1) (Addgene #17452, gift from Eric Campeau & Paul Kaufman) (Campeau et al., 2009) using NEBuilder HiFi DNA Assembly Master Mix (New England BioLabs). Lentivirus was produced in HEK293FT and collected 48h post-transfection. KO cells were transduced with filtered, lentivirus containing supernatant under addition of polybrene and selected using 4 μg/ml puromycin for 3-4 days. For PAPD5 and PAPD7, pCI3 plasmids with WT or catalytic mutant cDNA sequences were kindly provided by V. Narry Kim (Lim et al., 2018). For transient complementation, plasmids were transfected into WT or DKO cells using TransIT-LT1 Transfection Reagent (Mirus Bio), and transfected cells were plated in 96-wells the next day for HAV infection. To generate stable cell lines, cDNA sequences were cloned into the PB-CMV-MCS-EF1 α-Puro vector (PB510B-1, SBI System Biosciences) where the CMV promoter was replaced by a PGK promoter. Plasmids were co-transfected together with a plasmid expressing piggyBac transposase into *PAPD5* KO cells, which were subsequently selected with puromycin for 5 days starting 3 days post-transfection. All primer sequences can be found in Table S3.

Immunoblotting—Cell were lysed using Laemmli SDS sample buffer containing 5% beta-mercaptoethanol and boiled for 10 min. Lysates were separated by SDS-PAGE on pre-cast Bio-Rad 4%–15% poly-acrylamide gels in Bio-Rad Mini-Protean electrophoresis system. Proteins were transferred onto PVDF membranes using Bio-Rad Trans-Blot Turbo transfer system. PVDF membranes were blocked with PBS buffer containing 0.1% Tween-20 and 5% non-fat milk. Blocked membranes were incubated with primary antibody diluted in blocking buffer and incubated overnight at 4C on a shaker. Primary antibodies were detected by incubating membranes with 1:4000 dilution of HRP-conjugated (Southern Biotech) or 1:5000 dilution of IRDye-conjugated (LI-COR) secondary anti-mouse and anti-rabbit antibodies for 1 h at room temperature. Blots were visualized using a ChemiDoc MP Imaging System (Bio-Rad). The following primary antibodies (and their dilutions) were used in this study: p84 (Genetex, GTX70220) at 1:1000, GAPDH (SCBT, sc-32233) at 1:1000, vinculin (SCBT, sc-73614), 1:1000, eIF4B (SCBT, sc-376062) at 1:250, VPS4A (SCBT, sc-393428) at 1:300, SLC35A1 (Proteintech, 16342-1-AP) at 1:250, HAV VP1 (LS Bio, LS-C137674-100) at 1:1000, FLAG M2 (Sigma, F1804) at 1:1000, UFM1 (Abcam, ab109305) at 1:1000, UBA5 (Bethyl, A304-115A) at 1:2500, UFSP2 (SCBT, sc-376084) at 1:100, RPL26 (Bethyl, A300-686A) at 1:1000, PAPD5 (Atlas Antibodies, HPA042968) at 1:1000 and ZCCHC14 (Bethyl, A303-096A) at 1:1000. For SLC35A1, lysates from 10^6 cells were immunoprecipitated using 4 μg anti-SLC35A1 antibody and Protein G magnetic Dynabeads (Thermo Scientific, 10-003-D) overnight at 4C prior to immunoblotting to enhance signal and specificity of signal.

Immunoprecipitation—$1.5x10^6$ UFSP2 KO cells transduced with either WT-RPL26-FLAG or 5KR-RPL26-FLAG were washed with ice-cold PBS and lysed in 400 μL Pierce CoIP Lysis Buffer (ThermoFisher) containing Halt Protease inhibitor (ThermoFisher) on ice for 15 min. Lysates were centrifuged at 13,000xg at 4C for 10min, and supernatant was transferred to new tubes. For immunoprecipitation of FLAG-tagged RPL26, lysates were incubated with 25 μL Anti-FLAG M2 magnetic beads (Sigma) per condition overnight at 4C while rotating. Next day, beads were washed 3 times with TBS and FLAG-tagged RPL26 was eluted using 50 μL of 100 ng/μl FLAG peptide (Sigma) for 30 min on. Eluates were

mixed with Laemmli buffer containing 5% beta-mercaptoethanol, boiled for 10 min and analyzed by western blot as described above.

Replicon assay—The replicon plasmids pLuc-HAV/18f and pLuc-HAV/18f-3D^{pol}GDD→GAA (replication-defective mutant) were kindly provided by Stanley Lemon and were described previously (González-López et al., 2018). Plasmids were linearized using MluI-HF (New England BioLabs), RNA was generated using the MEGAscript T7 Kit (Invitrogen) and subsequently purified by lithium chloride precipitation. For electroporation, 1-2 million cells were washed three times in PBS, resuspended in 100 μL SF Nucleofector solution (Lonza), mixed with 250 ng replicon RNA per 80k cells, transferred to a 100 μL nucleocuvette and pulsed using the program FF-137 on an Amaxa 4D-Nucleofector X Unit (Lonza). Cells were then resuspended in equilibrated, antibiotic-free medium, distributed into 96-wells and lysed at different time points post-electroporation using 40 μL Passive Lysis buffer (Promega). Luminescence was measured using Luciferase Assay System (Promega) on a white-walled luminescence plate with an EnVision plate reader (PerkinElmer).

Poly(A) tail length assay by polyacrylamide gel electrophoresis—Cells were infected with HAV HM175/18f (MOI = 10) and harvested 3 dpi using Trizol (Invitrogen). RNA was purified with Direct-zol RNA Microprep columns (Zymo). HAV poly(A) tails were analyzed using the Poly(A) Tail-Length Assay Kit (ThermoFisher) according to the manufacturer's instructions. Briefly, 1 μg total RNA per condition was used as input for G/I tailing reaction followed by reverse transcription. Next, RT products were amplified using either the genome-specific (GS) forward and GS reverse primer, or GS forward and G/I specific reverse primer. PCR products were analyzed using polyacrylamide gel electrophoresis on a 5% Mini-PROTEAN Tris/Boric Acid/EDTA(TBE) gel in TBE buffer (100V for 60min). Gel was stained with SYBR Gold (diluted 1:10000 in TBE buffer) for ~30min in the dark and imaged on a ChemiDoc MP Imaging System (Bio-Rad).

Poly(A) tail sequencing—RNA was isolated from infected cells as described above. Ribosomal RNA (rRNA) was depleted from 1 μg total RNA by addition of rRNA Removal Mix – Gold (Illumina) followed by incubation at 68C for 5min, addition of rRNA Removal Beads (Illumina), removal of supernatant while tubes are on a magnetic rack, and finally elution of rRNA-depleted RNA. Next, a 5′ adenylated, 3′ blocked oligodeoxynucleotide RNA linker (S1315S, New England BioLabs) was ligated to the 3′ ends of RNAs by incubation with RNA ligase 2, truncated (New England BioLabs) for 3h at 22C. Ligation products were then reverse transcribed using a primer, which is reverse complement to the RNA linker, and Superscript IV (Invitrogen). Finally, HAV poly(A) tails were specifically amplified in a nested PCR, cloned into the pCRBlunt II-TOPO vector (Invitrogen) and Sanger sequenced (Quintarabio). Number of adenosines downstream of the HAV 3′UTR region and occurrence of non-adenosine nucleotides were counted.

Tapestation analysis of poly(A) tails of replicon RNA—10^6 cells were electroporated with *in-vitro* transcribed replicon RNA containing a 40bp long poly(A) tail as described above. For each time point, cells were washed with PBS, trypsinized, pelleted,

and lysed using Trizol followed by RNA extraction with Direct-zol columns. Total RNA was G/I tailed, reverse transcribed and poly(A) tail region was amplified using the GS forward primer and G/I reverse primer. Products were analyzed using a High Sensitivity D1000 ScreenTape System (Agilent).

Northern blot assay—For detection of HAV RNA from infected cells, cells were lysed in Trizol (ThermoFisher) and total RNA was purified by Trizol/chloroform extraction. Samples containing 5 μg of RNA and RNA loading dye were incubated at 65C for 15 min, then put immediately on ice before loading into a 1% denaturing formaldehyde-agarose gel from the NorthernMax kit (ThermoFisher) and containing SYBRSafe (Invitrogen). RNA was separated by gel electrophoresis in MOPS buffer at 90V. Gel was visualized for total RNA on ChemiDoc MP Imaging System (Bio-Rad). Gel was then transferred onto BrightStar-Plus Positively Charged Nylon Membrane (ThermoFisher) by passive downward capillary transfer for 2h using transfer buffer from the NorthernMax kit (ThermoFisher) and nylon membrane was subsequently UV-crosslinked with 1200J by the UV Stratalinker1800 (Stratagene). Membrane was pre-hybridized for 1h at 68C with NorthernMax Hybridization buffer and then hybridized overnight at same temperature with 25ng/ml of an HAV-specific DIG-labeled antisense RNA probe. The HAV antisense probe was generated by cloning the nucleotides 7118-7465 of the HAV/18f genome (GenBank: KP879216) into the pCR-BluntII vector and T7 *in-vitro* transcription from linearized plasmid using the DIG Northern Starter Kit (Roche). After overnight hybridization, membranes were washed, blocked, and incubated with anti-digoxigenin-AP Fab fragments from the DIG Northern Starter Kit (Roche) according to the manufacturer's instructions. Images were acquired with the ChemiDoc MP Imaging System (Bio-Rad).

To measure HAV RNA stability by Northern blot, 4 million WT or DKO Huh7.5.1 cells were electroporated with 12.5 μg of HAV replication-deficient replicon RNA each using SF Nucleofector solution (Lonza) and the program FF-137 on an Amaxa 4D-Nucleofector X Unit (Lonza). Cells were harvested at different time points by washing twice with PBS and lysis in Trizol. Extraction of total RNA and Northern blot analysis was performed as described above.

For the oligo(dT)/RNase H-Northern blot assay, 7.5 μg of total RNA from infected WT or DKO Huh7.5.1 cells collected at 72 hpi was mixed with 20 μl of 10 μM HAV-specific antisense oligo (targeting nucleotides 7080-7100 of the HAV/18f genome) and with or without 16.7 μl of 50 μM oligo$(dT)_{20}$. Reaction mix was incubated at 85C for 2min, then 42C for 10min and slowly cooled down to 32C. 4 μl RNase H (New England Biolabs) and 2 μl RNase inhibitor were added and reaction was incubated at 37C for 1h. Reactions were cleaned up using RNA Clean & Concentrator (Zymo) and equal amounts of RNA were denatured with RNA loading dye and loaded onto a formaldehyde-agarose gel. Gel was run at 100Vfor 90min to achieve maximum resolution and Northern blot was performed as described above. Maximum exposure of 2h on ChemiDoc MP Imaging System (Bio-Rad) was taken for RNA signal from DKO samples.

Cell viability assay—Huh7.5.1 cells were treated with different concentrations of RG7834 for 3 days and viability was measured using Cell Titer Glo (Promega) according to the manufacturer's instructions.

Culture and HAV infection of human liver organoids—Bi-potent stem cell organoids were generated as previously described (Broutier et al., 2016; Huch et al., 2015). Briefly, liver tissue samples from healthy resection margins of partial hepatectomies were obtained through the Ibrahim El-Hefni Liver Biorepository at the California Pacific Medical Center Research Institute. Following tissue digest, the heterogeneous mixture of single cells was suspended in reduced growth factor BME2 (Basement Membrane Extract, Type 2, Trevigen). From this mixture, 50 μL drops containing 1,000 to 20,000 cells were seeded in 24-well suspension culture plates (GreinerBio). Drops were incubated at 37C for > 20 min and solidified. After this, 500 μL of expansion media (EM) was added to each well. Expansion media is basal media (Advanced DMEM/F12 with 1% penicillin/streptomycin, 1% Glutamax, and 10 mM HEPES (all from ThermoFisher) supplemented with 1% N2 (GIBCO), 1% B27 (GIBCO), 1 mM N-Acetylcysteine (Sigma-Aldrich), 10 nM [Leu^{15}]-gastrin I human (Sigma-Aldrich), 10% (vol/vol) R-spondin1 conditioned media (generated as described in Broutier et al., 2016)), and 10 mM Nicotinamide (Sigma-Aldrich). Expansion media additionally contains 50 ng/ml recombinant human EGF, 25 ng/ml recombinant human HGF, 100 ng/ml recombinant human FGF10, 10 μM Forskolin, and 5 μM A83-01 (all from Stem Cell Technologies). Expansion media was replaced every 3-4 days. Organoids in expansion media grew in culture for 4-6 months and needed to be routinely passaged with TRYPLE (GIBCO). To induce differentiation to a hepatocyte-like fate, expansion media was supplemented with 25 ng/ml BMP7 (ProSpec) for 3-4 days. After this, media was changed to differentiation media (DM). Differentiation media is basal media supplemented with 1% N2, 1% B27, 1 mM N-acetylcysteine, 10 nM [Leu^{15}]-gastrin I human, 50 ng/ml EGF, 25 ng/ml HGF, 0.5 μM A83-01, 25 ng/ml BMP7, 3 μM dexamethasone (Sigma-Aldrich), 10 μM DAPT (Stem Cell Technologies), and 100 ng/ml recombinant human FGF19 (ProSpec). Differentiation media was changed every 3-4 days for a period of 3-15 days. For HAV infection, organoid lines from two non-viral donors were spin-infected with the HM175/18f strain of HAV as follows. Organoids from EM and DM d3 conditions were collected and lightly dissociated by a 3 min incubation at 37°C with TRYPLE. Cells were then suspended in basal media containing 10 μM Y-27632 (Stem Cell Technologies) and counted. These cells were mixed with HAV at an MOI of 500 focus forming units/cell in the presence and absence of RG7834 at 100 or 500 nM. Cell suspensions were then added to a 24-well suspension culture plate. The plate was centrifuged at 600 x g for 1 h at room temperature, followed by a 2 h incubation at 37C. After this, cells were collected and washed 3x in basal media. Washed cells were seeded in fresh BME2 drops in a new 24-well suspension culture plate. At 7 days post-infection, infected organoid samples were washed 2x in cold basal media, and cell pellets were lysed in Trizol.

QUANTIFICATION AND STATISTICAL ANALYSIS

For viral infection, drug treatment, and cell viability experiments biological replicates are defined as independent treatments and measurements from cells separately plated in and

harvested from multiple wells. Replicates are displayed as mean ± s.e.m. or mean ± s.d. as specified in the figure legends. Mean ± s.e.m. for qRT-PCR data was determined using CFX Maestro Software (Bio-Rad) and then visualized in GraphPad Prism 8. Mean ± s.e.m. or mean ± s.d. for remaining data was calculated and visualized using GraphPad Prism 8. Statistical tests were performed using GraphPad Prism 8 and p value definitions are listed in the figure legends.

Supplementary Material

Refer to Web version on PubMed Central for supplementary material.

ACKNOWLEDGMENTS

We would like to thank Don Ganem for helpful discussions and critically reading the manuscript, Sandra Schmid for valuable feedback on the manuscript, the Biohub Genomics platform for help with sequencing, James Webber for assistance with the CRISPR screen analysis, and members of the Biohub Infectious Disease Initiative for helpful discussions. We would like to acknowledge Drs. Stanley Lemon (University of North Carolina, Chapel Hill), Jan Carette (Stanford University), V. Narry Kim (Seoul National University), Ron Kopito(Stanford University), Ulrike Protzer (Technical University Munich), Feng Zhang (Broad Institute), Christoph Seeger (Fox Chase Cancer Center), and Suzanne Emerson (NIH) for providing critical reagents. We also acknowledge Drs. Stewart Cooper and Ann Erickson, who oversee the Ibrahim El-Hefni Liver Biorepository at the California Pacific Medical Center Research Institute and provided patient tissue samples used to generate liver organoids. The research was funded by the Chan Zuckerberg Biohub (A.S.P.) and by NIH/NIAID grant R01AI097552 and NIH/NIDA grant DP1DA038043-01 (M.O.). N.L.M. was supported in part by NIH/NIDDK grant T32DK060414.

REFERENCES

Ali IK, McKendrick L, Morley SJ, and Jackson RJ (2001). Activity of the hepatitis A virus IRES requires association between the cap-binding translation initiation factor (eIF4E) and eIF4G. J. Virol 75, 7854–7863. [PubMed: 11483729]

Avanzino BC, Fuchs G, and Fraser CS (2017). Cellular cap-binding protein, eIF4E, promotes picornavirus genome restructuring and translation. Proc. Natl. Acad. Sci. USA 114, 9611–9616. [PubMed: 28827335]

Baggen J, Thibaut HJ, Staring J, Jae LT, Liu Y, Guo H, Slager JJ, de Bruin JW, van Vliet ALW, Blomen VA, et al. (2016). Enterovirus D68 receptor requirements unveiled by haploid genetics. Proc. Natl. Acad. Sci. USA 113, 1399–1404. [PubMed: 26787879]

Bergamini G, Preiss T, and Hentze MW (2000). Picornavirus IRESes and the poly(A) tail jointly promote cap-independent translation in a mammalian cell-free system. RNA 6, 1781–1790. [PubMed: 11142378]

Berndt H, Harnisch C, Rammelt C, Stöhr N, Zirkel A, Dohm JC, Himmelbauer H, Tavanez J-P, Hüttelmaier S, and Wahle E (2012). Maturation of mammalian H/ACA box snoRNAs: PAPD5-dependent adenylation and PARN-dependent trimming. RNA 18, 958–972. [PubMed: 22442037]

Boele J, Persson H, Shin JW, Ishizu Y, Newie IS, S×kilde R, Hawkins SM, Coarfa C, Ikeda K, Takayama K, et al. (2014). PAPD5-mediated 3′ adenylation and subsequent degradation of miR-21 is disrupted in proliferative disease. Proc. Natl. Acad. Sci. USA 111, 11467–11472. [PubMed: 25049417]

Borman AM, and Kean KM (1997). Intact eukaryotic initiation factor 4G is required for hepatitis A virus internal initiation of translation. Virology 237, 129–136. [PubMed: 9344915]

Broutier L, Andersson-Rolf A, Hindley CJ, Boj SF, Clevers H, Koo B-K, and Huch M (2016). Culture and establishment of self-renewing human and mouse adult liver and pancreas 3D organoids and their genetic manipulation. Nat. Protoc 11, 1724–1743. [PubMed: 27560176]

Campeau E, Ruhl VE, Rodier F, Smith CL, Rahmberg BL, Fuss JO, Campisi J, Yaswen P, Cooper PK, and Kaufman PD (2009). A versatile viral system for expression and depletion of proteins in mammalian cells. PLoS ONE 4, e6529. [PubMed: 19657394]

CDC (2019). Widespread person-to-person outbreaks of hepatitis A across the United States. https://www.cdc.gov/hepatitis/outbreaks/2017March-HepatitisA.htm.

Chen C, Itakura E, Weber KP, Hegde RS, and de Bono M (2014). An ER complex of ODR-4 and ODR-8/Ufm1 specific protease 2 promotes GPCR maturation by a Ufm1-independent mechanism. PLoS Genet. 10, e1004082. [PubMed: 24603482]

Chen J-H, Zhang R-H, Lin S-L, Li P-F, Lan J-J, Song S-S, Gao J-M, Wang Y, Xie Z-J, Li F-C, and Jiang SJ (2018). The Functional Role of the 3′ Untranslated Region and Poly(A) Tail of Duck Hepatitis A Virus Type 1 in Viral Replication and Regulation of IRES-Mediated Translation. Front. Microbiol 9, 2250. [PubMed: 30319572]

Das A, Hirai-Yuki A, González-López O, Rhein B, Moller-Tank S, Brouillette R, Hensley L, Misumi I, Lovell W, Cullen JM, et al. (2017). TIM1 (HAVCR1) Is Not Essential for Cellular Entry of Either Quasi-enveloped or Naked Hepatitis A Virions. MBio 8, 8.

Das A, Barrientos R, Shiota T, Madigan V, Misumi I, McKnight KL, Sun L, Li Z, Meganck RM, Li Y, et al. (2020). Gangliosides are essential endosomal receptors for quasi-enveloped and naked hepatitis A virus. Nat. Microbiol 5, 1069–1078. [PubMed: 32451473]

Diep J, Ooi YS, Wilkinson AW, Peters CE, Foy E, Johnson JR, Zengel J, Ding S, Weng K-F, Laufman O, et al. (2019). Enterovirus pathogenesis requires the host methyltransferase SETD3. Nat. Microbiol 4,2523–2537. [PubMed: 31527793]

Ding S, Diep J, Feng N, Ren L, Li B, Ooi YS, Wang X, Brulois KF, Yasukawa LL, Li X, et al. (2018). STAG2 deficiency induces interferon responses via cGAS-STING pathway and restricts virus infection. Nat. Commun 9, 1485. [PubMed: 29662124]

Drake MJ, Brennan B Jr., Briley K Jr., Bart SM, Sherman E, Szemiel AM, Minutillo M, Bushman FD, and Bates P (2017). A role for glycolipid biosynthesis in severe fever with thrombocytopenia syndrome virus entry. PLoS Pathog. 13, e1006316. [PubMed: 28388693]

Eden E, Navon R, Steinfeld I, Lipson D, and Yakhini Z (2009). GOrilla: a tool for discovery and visualization of enriched GO terms in ranked gene lists. BMC Bioinformatics 10, 48. [PubMed: 19192299]

Feng Z, Hensley L, McKnight KL, Hu F, Madden V, Ping L, Jeong S-H, Walker C, Lanford RE, and Lemon SM (2013). A pathogenic picornavirus acquires an envelope by hijacking cellular membranes. Nature 496, 367–371. [PubMed: 23542590]

Feng Z, Hirai-Yuki A, McKnight KL, and Lemon SM (2014). Naked Viruses That Aren't Always Naked: Quasi-Enveloped Agents of Acute Hepatitis. Annu. Rev. Virol 1, 539–560. [PubMed: 26958733]

Gerakis Y, Quintero M, Li H, and Hetz C (2019). The UFMylation System in Proteostasis and Beyond. Trends Cell Biol. 29, 974–986. [PubMed: 31703843]

González-López O, Rivera-Serrano EE, Hu F, Hensley L, McKnight KL, Ren J, Stuart DI, Fry EE, and Lemon SM (2018). Redundant Late Domain Functions of Tandem VP2 YPX_3L Motifs in Nonlytic Cellular Egress of Quasi-enveloped Hepatitis A Virus. J. Virol 92, 92.

Gosert R, Chang KH, Rijnbrand R, Yi M, Sangar DV, and Lemon SM (2000). Transient expression of cellular polypyrimidine-tract binding protein stimulates cap-independent translation directed by both picornaviral and flaviviral internal ribosome entry sites In vivo. Mol. Cell. Biol 20, 1583–1595. [PubMed: 10669736]

Graff J, Cha J, Blyn LB, and Ehrenfeld E (1998). Interaction of poly(rC) binding protein 2 with the 5′ noncoding region of hepatitis A virus RNA and its effects on translation. J. Virol 72, 9668–9675. [PubMed: 9811700]

Ha BH, Jeon YJ, Shin SC,Tatsumi K, Komatsu M, Tanaka K, Watson CM, Wallis G, Chung CH, and Kim EE (2011). Structure of ubiquitin-fold modifier 1-specific protease UfSP2. J. Biol. Chem 286, 10248–10257. [PubMed: 21228277]

Hamill S, Wolin SL, and Reinisch KM (2010). Structure and function of the polymerase core of TRAMP, a RNA surveillance complex. Proc. Natl. Acad. Sci. USA 107, 15045–15050. [PubMed: 20696927]

Han J, Perez JT, Chen C, Li Y, Benitez A, Kandasamy M, Lee Y, Andrade J, tenOever B, and Manicassamy B (2018). Genome-wide CRISPR/Cas9 Screen Identifies Host Factors Essential for Influenza Virus Replication. Cell Rep. 23, 596–607. [PubMed: 29642015]

Hsiau T, Conant D, Rossi N, Maures T, Waite K, Yang J, Joshi S, Kelso R, Holden K, Enzmann BL, et al. (2019). Inference of CRISPR Edits from Sanger Trace Data. BioRxiv, 251082.

Huang S-W, Wang Y-F, Yu C-K, Su I-J, and Wang J-R (2012). Mutations in VP2 and VP1 capsid proteins increase infectivity and mouse lethality of enterovirus 71 by virus binding and RNA accumulation enhancement. Virology 422, 132–143. [PubMed: 22078110]

Huch M, Gehart H, van Boxtel R, Hamer K, Blokzijl F, Verstegen MMA, Ellis E, van Wenum M, Fuchs SA, de Ligt J, et al. (2015). Long-term culture of genome-stable bipotent stem cells from adult human liver. Cell 160, 299–312. [PubMed: 25533785]

Hyrina A, Jones C, Chen D, Clarkson S, Cochran N, Feucht P, Hoffman G, Lindeman A, Russ C, Sigoillot F, et al. (2019). A Genome-wide CRISPR Screen Identifies ZCCHC14 as a Host Factor Required for Hepatitis B Surface Antigen Production. Cell Rep. 29, 2970–2978.e6. [PubMed: 31801065]

Jacobsen KH (2018). Globalization and the Changing Epidemiology of Hepatitis A Virus. Cold Spring Harb. Perspect. Med 8, a031716. [PubMed: 29500305]

Jha S, Rollins MG, Fuchs G, Procter DJ, Hall EA, Cozzolino K, Sarnow P, Savas JN, and Walsh D (2017). Trans-kingdom mimicry underlies ribosome customization by a poxvirus kinase. Nature 546, 651–655. [PubMed: 28636603]

Jiang X, Kanda T, Wu S, Nakamoto S, Saito K, Shirasawa H, Kiyohara T, Ishii K, Wakita T, Okamoto H, and Yokosuka O (2014). Suppression of La antigen exerts potential antiviral effects against hepatitis A virus. PLoS ONE 9, e101993. [PubMed: 24999657]

Kang SH, Kim GR, Seong M, Baek SH, Seol JH, Bang OS, Ovaa H, Tatsumi K, Komatsu M, Tanaka K, and Chung CH (2007). Two novel ubiquitin-fold modifier 1 (Ufm1)-specific proteases, UfSP1 and UfSP2. J. Biol. Chem 282, 5256–5262. [PubMed: 17182609]

Kaplan G, Totsuka A, Thompson P, Akatsuka T, Moritsugu Y, and Feinstone SM (1996). Identification of a surface glycoprotein on African green monkey kidney cells as a receptor for hepatitis A virus. EMBO J. 15, 4282–4296. [PubMed: 8861957]

Kempf BJ, Kelly MM, Springer CL, Peersen OB, and Barton DJ (2013). Structural features of a picornavirus polymerase involved in the polyadenylation of viral RNA. J. Virol 87, 5629–5644. [PubMed: 23468507]

Kim D, Lee YS, Jung S-J, Yeo J, Seo JJ, Lee Y-Y, Lim J, Chang H, Song J, Yang J, et al. (2020). Viral hijacking of the TENT4-ZCCHC14 complex protects viral RNAs via mixed tailing. Nat. Struct. Mol. Biol 27, 581–588. [PubMed: 32451488]

Ko C, Chakraborty A, Chou W-M, Hasreiter J, Wettengel JM, Stadler D, Bester R, Asen T, Zhang K, Wisskirchen K, et al. (2018). Hepatitis B virus genome recycling and de novo secondary infection events maintain stable cccDNA levels. J. Hepatol 69, 1231–1241. [PubMed: 30142426]

Komatsu M, Chiba T, Tatsumi K, Iemura S, Tanida I, Okazaki N, Ueno T, Kominami E, Natsume T, and Tanaka K (2004). A novel protein-conjugating system for Ufm1, a ubiquitin-fold modifier. EMBO J. 23, 1977–1986. [PubMed: 15071506]

Ladner SK, Otto MJ, Barker CS, Zaifert K, Wang GH, Guo JT, Seeger C, and King RW (1997). Inducible expression of human hepatitis B virus (HBV) in stably transfected hepatoblastoma cells: a novel system for screening potential inhibitors of HBV replication. Antimicrob. Agents Chemother 41, 1715–1720. [PubMed: 9257747]

Landry DM, Hertz MI, and Thompson SR (2009). RPS25 is essential for translation initiation by the Dicistroviridae and hepatitis C viral IRESs. Genes Dev. 23, 2753–2764. [PubMed: 19952110]

Lemon SM, Murphy PC, Shields PA, Ping LH, Feinstone SM, Cromeans T, and Jansen RW (1991). Antigenic and genetic variation in cytopathic hepatitis A virus variants arising during persistent infection: evidence for genetic recombination. J. Virol 65, 2056–2065. [PubMed: 1705995]

Li W, Xu H, Xiao T, Cong L, Love MI, Zhang F, Irizarry RA, Liu JS, Brown M, and Liu XS (2014). MAGeCK enables robust identification of essential genes from genome-scale CRISPR/Cas9 knockout screens. Genome Biol. 15, 554. [PubMed: 25476604]

Liang JR, Lingeman E, Luong T, Ahmed S, Muhar M, Nguyen T, Olzmann JA, and Corn JE (2020). A Genome-wide ER-phagy Screen Highlights Key Roles of Mitochondrial Metabolism and ER-Resident UFMylation. Cell 180, 1160–1177.e20. [PubMed: 32160526]

Lim J, Kim D, Lee Y-S, Ha M, Lee M, Yeo J, Chang H, Song J, Ahn K, and Kim VN (2018). Mixed tailing by TENT4A and TENT4B shields mRNA from rapid deadenylation. Science 361, 701–704. [PubMed: 30026317]

Lubas M, Christensen MS, Kristiansen MS, Domanski M, Falkenby LG, Lykke-Andersen S, Andersen JS, Dziembowski A, and Jensen TH (2011). Interaction profiling identifies the human nuclear exosome targeting complex. Mol. Cell 43, 624–637. [PubMed: 21855801]

Luo B, Cheung HW, Subramanian A, Sharifnia T, Okamoto M, Yang X, Hinkle G, Boehm JS, Beroukhim R, Weir BA, et al. (2008). Highly parallel identification of essential genes in cancer cells. Proc. Natl. Acad. Sci. USA 105, 20380–20385. [PubMed: 19091943]

Majzoub K, Hafirassou ML, Meignin C, Goto A, Marzi S, Fedorova A, Verdier Y, Vinh J, Hoffmann JA, Martin F, et al. (2014). RACK1 controls IRES-mediated translation of viruses. Cell 159, 1086–1095. [PubMed: 25416947]

Marceau CD, Puschnik AS, Majzoub K, Ooi YS, Brewer SM, Fuchs G, Swaminathan K, Mata MA, Elias JE, Sarnow P, and Carette JE (2016). Genetic dissection of Flaviviridae host factors through genome-scale CRISPR screens. Nature 535, 159–163. [PubMed: 27383987]

McKnight KL, and Lemon SM (2018). Hepatitis A Virus Genome Organization and Replication Strategy. Cold Spring Harb. Perspect. Med 8, 033480.

Mueller H, Wildum S, Luangsay S, Walther J, Lopez A, Tropberger P, Ottaviani G, Lu W, Parrott NJ, Zhang JD, et al. (2018). A novel orally available small molecule that inhibits hepatitis B virus expression. J. Hepatol 68,412–420. [PubMed: 29079285]

Mueller H, Lopez A, Tropberger P, Wildum S, Schmaler J, Pedersen L, Han X, Wang Y, Ottosen S, Yang S, et al. (2019). PAPD5/7 Are Host Factors That Are Required for Hepatitis B Virus RNA Stabilization. Hepatology 69, 1398–1411. [PubMed: 30365161]

Nousch M, Yeroslaviz A, Habermann B, and Eckmann CR (2014). The cytoplasmic poly(A) polymerases GLD-2 and GLD-4 promote general gene expression via distinct mechanisms. Nucleic Acids Res. 42, 11622–11633. [PubMed: 25217583]

Pestova TV, Hellen CU, and Shatsky IN (1996). Canonical eukaryotic initiation factors determine initiation of translation by internal ribosomal entry. Mol. Cell. Biol 16, 6859–6869. [PubMed: 8943341]

Rammelt C, Bilen B, Zavolan M, and Keller W (2011). PAPD5, a noncanonical poly(A) polymerase with an unusual RNA-binding motif. RNA 17, 1737–1746. [PubMed: 21788334]

Ran FA, Hsu PD, Wright J,Agarwala V, Scott DA, and Zhang F (2013). Genome engineering using the CRISPR-Cas9 system. Nat. Protoc 8, 2281–2308. [PubMed: 24157548]

Rivera-Serrano EE, González-López O, Das A, and Lemon SM (2019). Cellular entry and uncoating of naked and quasi-enveloped human hepatoviruses. eLife 8, e43983. [PubMed: 30801249]

Sallés FJ, Richards WG, and Strickland S (1999). Assaying the polyadenylation state of mRNAs. Methods 17, 38–45. [PubMed: 10075881]

Sanjana NE, Shalem O, and Zhang F (2014). Improved vectors and genome-wide libraries for CRISPR screening. Nat. Methods 11, 783–784. [PubMed: 25075903]

Shcherbik N, Wang M, Lapik YR, Srivastava L, and Pestov DG (2010). Polyadenylation and degradation of incomplete RNA polymerase I transcripts in mammalian cells. EMBO Rep. 11, 106–111. [PubMed: 20062005]

Shin J, Paek KY, Ivshina M, Stackpole EE, and Richter JD (2017). Essential role for non-canonical poly(A) polymerase GLD4 in cytoplasmic polyadenylation and carbohydrate metabolism. Nucleic Acids Res. 45, 6793–6804. [PubMed: 28383716]

Shukla P, Nguyen HT, Faulk K, Mather K, Torian U, Engle RE, and Emerson SU (2012). Adaptation of a genotype 3 hepatitis E virus to efficient growth in cell culture depends on an inserted human gene segment acquired by recombination. J. Virol 86, 5697–5707. [PubMed: 22398290]

Spector DH, and Baltimore D (1975). Polyadenylic acid on poliovirus RNA IV. Poly(U) in replicative intermediate and double-stranded RNA. Virology 67, 498–505. [PubMed: 171838]

Steil BP, Kempf BJ, and Barton DJ (2010). Poly(A) at the 3′ end of positive-strand RNA and VPg-linked poly(U) at the 5′ end of negative-strand RNA are reciprocal templates during replication of poliovirus RNA. J. Virol 84, 2843–2858. [PubMed: 20071574]

Tatsumi K, Sou YS, Tada N, Nakamura E, Iemura S, Natsume T, Kang SH, Chung CH, Kasahara M, Kominami E, et al. (2010). A novel type of E3 ligase for the Ufm1 conjugation system. J. Biol. Chem 285, 5417–5427. [PubMed: 20018847]

Vanácová S, Wolf J, Martin G, Blank D, Dettwiler S, Friedlein A, Langen H, Keith G, and Keller W (2005). A new yeast poly(A) polymerase complex involved in RNA quality control. PLoS Biol. 3, e189. [PubMed: 15828860]

Votteler J, and Sundquist WI (2013). Virus budding and the ESCRT pathway. Cell Host Microbe 14, 232–241. [PubMed: 24034610]

Wakita T, Pietschmann T, Kato T, Date T, Miyamoto M, Zhao Z, Murthy K, Habermann A, Kräusslich H-G, Mizokami M, et al. (2005). Production of infectious hepatitis C virus in tissue culture from a cloned viral genome. Nat. Med 11, 791–796. [PubMed: 15951748]

Walczak CP, Leto DE, Zhang L, Riepe C, Muller RY, DaRosa PA, Ingolia NT, Elias JE, and Kopito RR (2019). Ribosomal protein RPL26 is the principal target of UFMylation. Proc. Natl. Acad. Sci. USA 116, 1299–1308. [PubMed: 30626644]

Wang L, Xu Y, Rogers H, Saidi L, Noguchi CT, Li H, Yewdell JW, Guydosh NR, and Ye Y (2020). UFMylation of RPL26 links translocation-associated quality control to endoplasmic reticulum protein homeostasis. Cell Res. 30, 5–20. [PubMed: 31595041]

Warkocki Z, Liudkovska V, Gewartowska O, Mroczek S, and Dziembowski A (2018). Terminal nucleotidyl transferases (TENTs) in mammalian RNA metabolism. Philos. Trans. R. Soc. Lond. B Biol. Sci 373, 20180162. [PubMed: 30397099]

Wu J,Lei G, Mei M, Tang Y, and Li H(2010).A novel C53/LZAP-interacting protein regulates stability of C53/LZAP and DDRGK domain-containing Protein 1 (DDRGK1) and modulates NF-kappaB signaling. J. Biol. Chem 285, 15126–15136. [PubMed: 20228063]

Zhang R, Miner JJ, Gorman MJ, Rausch K, Ramage H, White JP, Zuiani A, Zhang P, Fernandez E, Zhang Q, et al. (2016). A CRISPR screen defines a signal peptide processing pathway required by flaviviruses. Nature 535, 164–168. [PubMed: 27383988]

Zhong J, Gastaminza P, Cheng G, Kapadia S, Kato T, Burton DR, Wieland SF, Uprichard SL, Wakita T, and Chisari FV (2005). Robust hepatitis C virus infection in vitro. Proc. Natl. Acad. Sci. USA 102, 9294–9299. [PubMed: 15939869]

Highlights

- A genome-wide CRISPR screen identifies host factors important for hepatitis A virus
- UFMylation of the ribosomal protein RPL26 enhances viral translation
- PAPD5/7-ZCCHC14 TRAMP-like complexes are important for hepatitis A virus
- Pharmacological inhibition of PAPD5/7 reduces hepatitis A virus replication

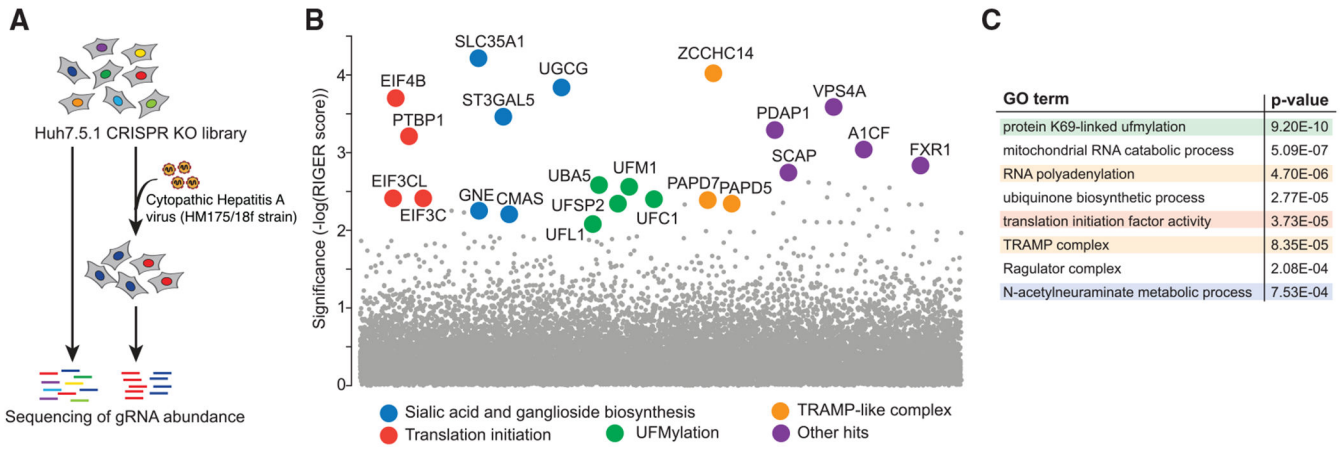

Figure 1. Genome-wide CRISPR KO screen identifies host cellular factors important for HAV infection

(A) Schematic of the genome-wide CRISPR KO screen. A library of Huh7.5.1-Cas9 CRISPR KO cells was infected with cytopathic HAV HM175/18f and virus-resistant cells were harvested 12 days post-infection (dpi). gRNA abundance was measured in the original and selected cell population by next-generation sequencing.

(B) Significance of enriched genes in CRISPR KO screen based on RIGER analysis. Hits were clustered and colored by function. The complete ranked gene list and RIGER scores can be found in Table S1.

(C) Selected terms from gene ontology (GO) analysis of genes enriched in CRISPR KO screen (RIGER $p < 0.001$). The complete list of GO terms can be found in Table S2.

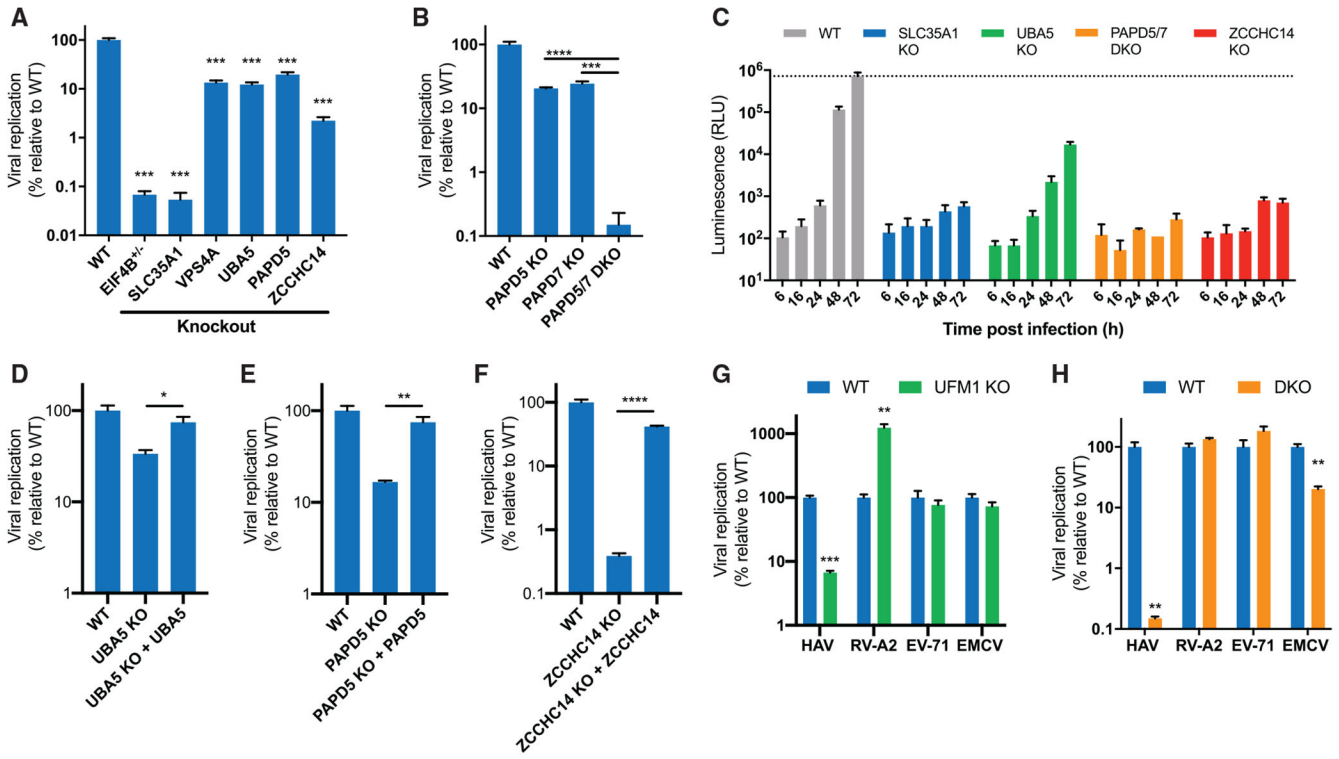

Figure 2. KO of identified host factor genes reduces HAV replication

(A) Quantification of HAV RNA in WT and clonal KO Huh7.5.1 cell lines by quantitative reverse transcriptase PCR (qRT-PCR) at 3 dpi. Of note, this time point likely supports multiple rounds of viral replication and spread.

(B) Quantification of HAV RNA in WT, *PAPD5* KO, *PAPD7* KO, and *PAPD5/PAPD7* double-KO (DKO) cells 3 dpi by qRT-PCR.

(C) Viral growth curves using recombinant HAV expressing nanoluciferase (HAV-Nluc). WT, *SLC35A1* KO, *UBA5* KO, *PAPD5/7* DKO, and *ZCCHC14* KO cells were infected and lysed at indicated time points, and luciferase levels were measured. Dotted line indicates luminescence levels in WT cells at 72 hpi. Data are displayed as mean ± SD (n = 3 biological replicates).

(D–F) Quantification of HAV RNA in WT, *UBA5* KO (D), *PAPD5* KO (E), or *ZCCHC14* KO (F) cells and KO cells complemented with respective cDNAs 3 dpi by qRT-PCR.

(G and H) Quantification of HAV, human rhinovirus A2 (RV-A2), enterovirus 71 (EV-71), and encephalomyocarditis virus (EMCV) RNA in WT versus *UFM1* KO cells (G) or WT versus DKO cells (H) by qRT-PCR. Cells infected with HAV or RV-A2 were harvested after 48 hpi, with EV-71 after 24 hpi and with EMCV after 8 hpi. For all qRT-PCR experiments, viral RNA was normalized to 18S RNA, and results are displayed relative to infection in WT cells.

Datasets represent mean ± SEM (n = 3 biological replicates). p values were determined by unpaired two-sided t tests using GraphPad Prism 8. *p < 0.05, **p < 0.01, ***p < 0.001, ****p < 0.0001.

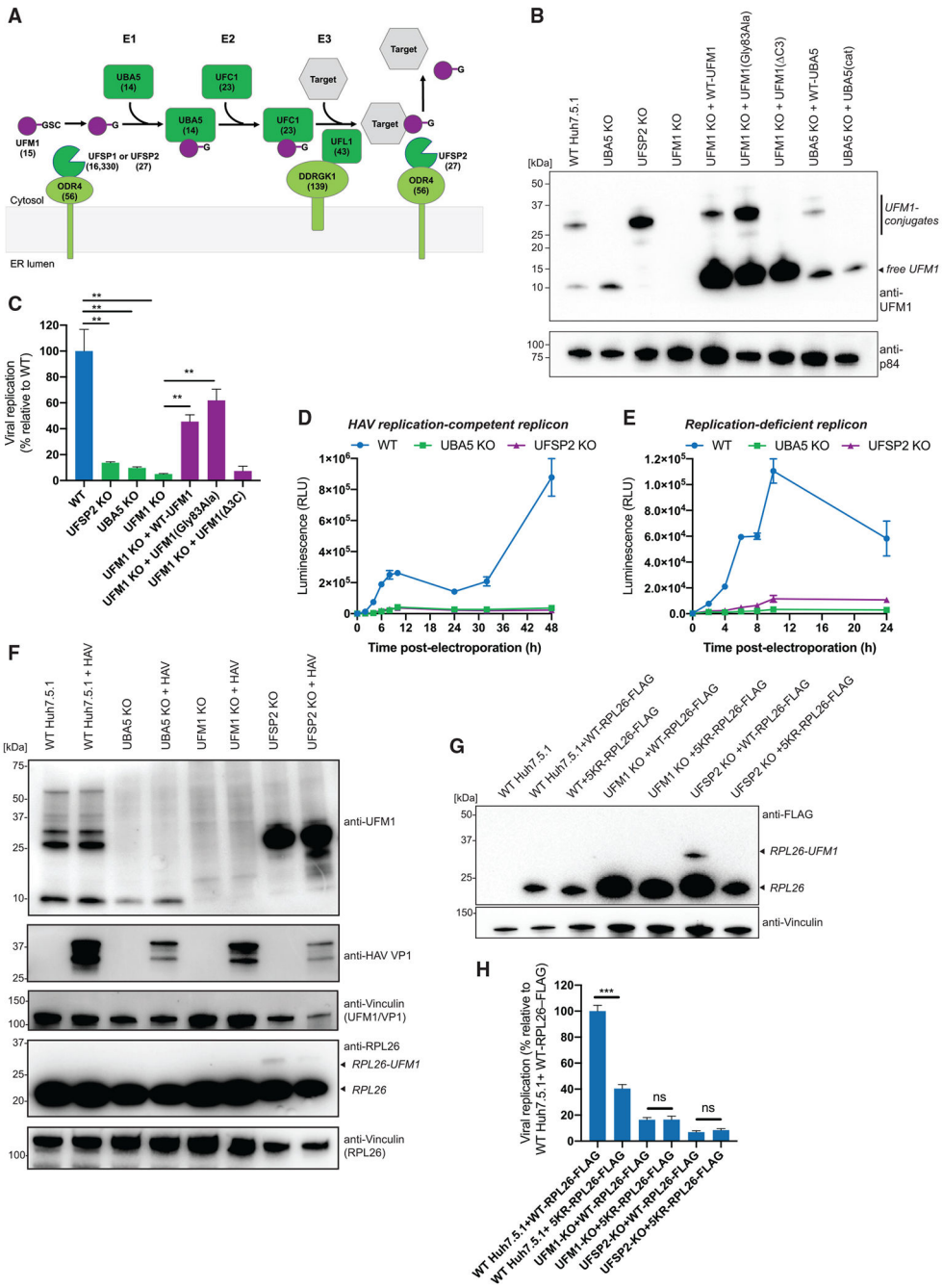

Figure 3. HAV depends on functional UFM1 conjugation of the ribosomal protein RPL26 for optimal translation

(A) Schematic of cellular UFMylation pathway. #, rank in gene enrichment analysis of CRISPR screen.

(B) UFM1 immunoblot of WT, *UBA5* KO, *UFSP2* KO, *UFM1* KO, and *UFM1* KO cells complemented with WT, Gly83Ala, or ΔC3 UFM1 as well as *UBA5* KO cells complemented with WT or catalytically inactive (cat) UBA5. Top bands represent UFM1 conjugation products, and the bottom band represents free UFM1. P84 was used as loading control.

(C) Quantification of HAV RNA in WT, *UFSP2* KO, *UBA5* KO, *UFM1* KO, and *UFM1* KO cells complemented with WT, Gly83Ala, or ΔC3 UFM1. Viral RNA was normalized to 18S RNA, and results are displayed relative to infection in WT cells.
(D) Time course of luciferase activity expressed by electroporated HAV-FLuc subgenomic replicon RNA in WT, *UBA5* KO, and *UFSP2* KO cells.
(E) Time course of luciferase activity expressed by electroporated HAV-FLuc subgenomic replication-incompetent replicon RNA in WT, *UBA5* KO, and *UFSP2* KO cells.
(F) Immunoblots of uninfected and HAV-infected WT, *UBA5* KO, *UFM1* KO, and *UFSP2* KO cells. Membranes were stained with anti-UFM1, anti-HAVVP1, or anti-RPL26 antibodies. Vinculin served as loading control.
(G) FLAG immunoblot of WT, *UFM1* KO, and *UFSP2* KO cells transduced with lentivirus expressing FLAG-tagged WT-RPL26 or 5KR-RPL26. Vinculin served as loading control.
(H) Quantification of HAV RNA in WT, *UFM1* KO, and *UFSP2* KO cells expressing WT-RPL26 or 5KR-RPL26. Viral RNA was normalized to 18S RNA and results are displayed relative to infection in WT cells expressing WT-RPL26.
For all qRT-PCR experiments, datasets represent mean ± SEM (n = 3 biological replicates). For luciferase experiments, datasets represent mean ± SD (n = 2 biological replicates)for each time point. p values were determined by unpaired two-sided t tests using GraphPad Prism 8. ns, non-significant; *p < 0.05, **p < 0.01, ***p < 0.001, ****p < 0.0001.

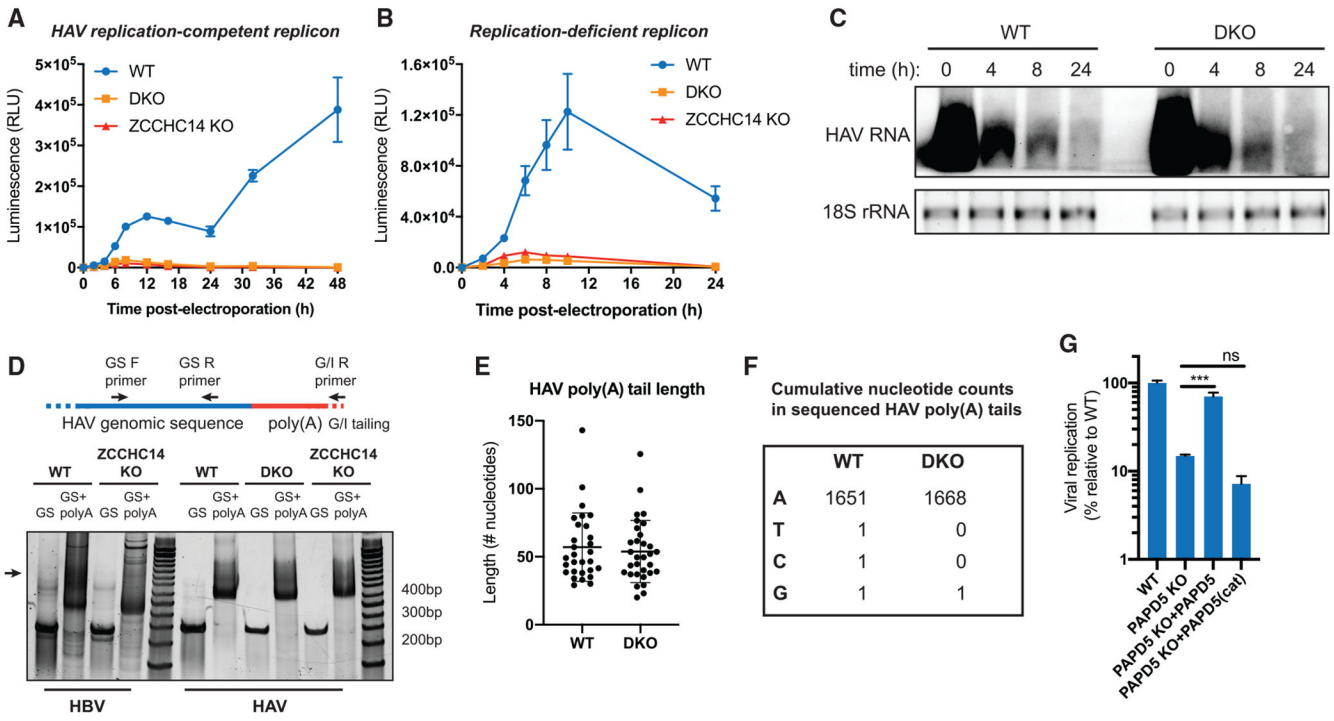

	WT	DKO
A	1651	1668
T	1	0
C	1	0
G	1	1

Figure 4. Catalytic activity of TRAMP-like complexes is important for HAV translation, independent of regulating viral poly(A) tail length or RNA stability

(A) Time course of luciferase activity expressed by electroporated HAV-FLuc subgenomic replicon RNA in WT, DKO and *ZCCHC14* KO cells. Datasets represent mean ± SD (n = 2 biological replicates) for each time point.

(B) Time course of luciferase activity expressed by electroporated HAV-FLuc replication-incompetent replicon RNA in WT, DKO cells, and *ZCCHC14* KO. Datasets represent mean ± SD (n = 2 biological replicates) for each time point.

(C) Northern blot of HAV RNA from WT or PAPD5/7 DKO cells, which were electroporated with replication-deficient HAV replicon and harvested at indicated time points post-electroporation. Membrane was stained using an *in vitro*-transcribed DIG-labeled anti-sense RNA probe targeting nucleotides 7118–7465 of the HAV genome. 18S ribosomal RNA was visualized using SYBR Safe dye on agarose gel prior to transfer onto membrane.

(D) Poly(A) tail length assay. Total RNA from infected WT or KO cells was G/I tailed at 3′ ends, reverse transcribed and PCR amplified by either genome-specific (GS) forward and GS reverse primers, or GS forward and G/I reverse primer. PCR products were analyzed by polyacrylamide gel electrophoresis. For HBV, total RNA was collected from infected WT or *ZCCHC14* KO HepG2-NTCP cells 14 dpi. For HAV, total RNA was harvested from infected WT, DKO, or *ZCCHC14* KO Huh7.5.1 cells 3 dpi. Arrow indicates a longer HBV poly(A) tail in WT cells.

(E) Length distribution of Sanger-sequenced HAV poly(A) tails. An RNA linker was ligated to 3′ ends of rRNA-depleted RNA from infected WT or DKO cells followed by reverse transcription and PCR amplification of the HAV poly(A) tail region. PCR products were TOPO cloned and Sanger sequenced.

(F) Analysis of nucleotide composition of sequenced HAV poly(A) tails from (E).
(G) Quantification of HAV RNA in WT, *PAPD5* KO, and *PAPD5* KO cells complemented with either WT or catalytically inactive (cat) PAPD5 cDNA 3 dpi by qRT-PCR. Viral RNA was normalized to 18S RNA, and results are displayed relative to infection in WT cells. Datasets represent mean ± SEM (n = 3 biological replicates). p values were determined by unpaired two-sided t tests using GraphPad Prism 8. ns, non-significant; ***$p < 0.001$.

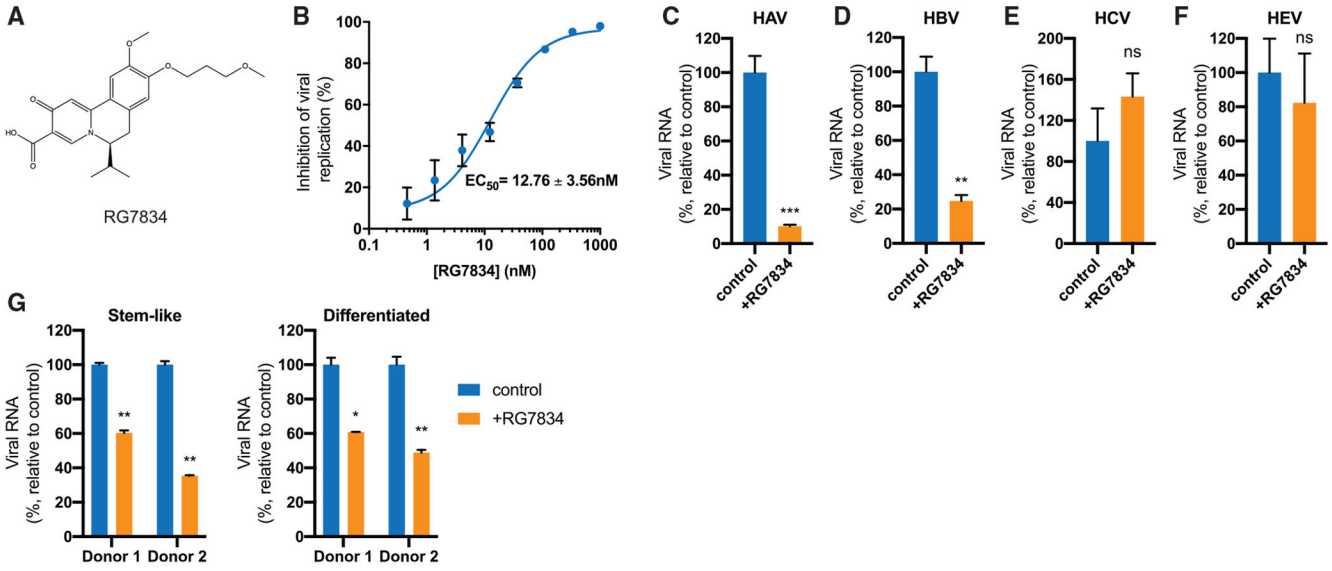

Figure 5. Small-molecule inhibition of PAPD5 and PAPD7 reduces HAV infection in human hepatocyte cells and human liver organoids

(A) Chemical structure of RG7834.

(B) Dose-response curve of HAV RNA levels in Huh7.5.1 cells treated with different RG7834 concentrations as measured by qRT-PCR 3 days post-infection/treatment. Non-linear curve was fitted with least-squares regression using GraphPad Prism 8, and EC_{50} was determined.

(C) Quantification of HAV RNA in control and RG7834 (100 nM)-treated Huh7.5.1 cells 3 dpi by qRT-PCR.

(D) Quantification of HBV total RNA in control and RG7834 (100 nM)-treated HepG2-NTCP cells 15 dpi by qRT-PCR. Drug was replenished every 3–4 days.

(E) Quantification of HCV RNA in control and RG7834 (100 nM)-treated Huh7.5.1 cells 3 dpi by qRT-PCR.

(F) Quantification of HEV RNA in control and RG7834 (100 nM)-treated Huh7.5.1 cells by qRT-PCR 6 days post-transfection of viral RNA.

(G) Quantification of HAV RNA in control and RG7834 (100 nM)-treated human liver organoids 7 dpi by qRT-PCR. Organoids were either stem-like or differentiated to adult hepatocytes prior to infection. For all qRT-PCR experiments, viral RNA was normalized to 18S RNA, and results are displayed relative to infection in control (DMSO) condition. Datasets in (B)–(F) represent mean ± SEM (n = 3 biological replicates). For organoid experiments (G), donor 1 and 2 represent 2 independent biological replicates, and qPCR was performed with 2 technical replicates. p values were determined by unpaired two-sided t tests using GraphPad Prism 8. ns, non-significant; *p < 0.05; **p < 0.01; ***p < 0.001.

KEY RESOURCES TABLE

REAGENT OR RESOURCE	SOURCE	IDENTIFIER
Antibodies		
p84	Genetex	Cat#GTX70220; RRID: AB_372637
GAPDH	Santa Cruz Biotechnology	Cat#sc-32233; RRID: AB_627679
Vinculin	Santa Cruz Biotechnology	Cat#sc-73614; RRID: AB_1131294
eIF4B	Santa Cruz Biotechnology	Cat#sc-376062; RRID: AB_10988946
VPS4A	Santa Cruz Biotechnology	Cat#sc-393428; RRID: AB_2773025
SLC35A1	Proteintech	Cat#16342-1-AP; RRID: AB_2190077
HAV VP1	Lifespan Biosciences	Cat#LS-C137674-100; RRID: AB_10948725
FLAG M2	Sigma-Aldrich	Cat#F1804; RRID: AB_262044
UFM1	Abcam	Cat#ab109305; RRID: AB_10864675
UBA5	Bethyl	Cat#A304-115A; RRID: AB_2621364
UFSP2	Santa Cruz Biotechnology	Cat#sc-376084; RRID: AB_10989729
RPL26	Bethyl	Cat#A300-686A; RRID: AB_530289
PAPD5	Atlas Antibodies	Cat#HPA042968 ; RRID: AB_267824
ZCCHC14	Bethyl	Cat#A303-096A ; RRID: AB_10895018
Goat Anti-Rabbit IgG-HRP	Southern Biotech	Cat#4030-05; RRID: AB_2687483
Goat anti-Mouse-HRP	Southern Biotech	Cat#1031-05; RRID: AB_2794307
Goat anti-Rabbit IRDye 800CW	LI-COR	Cat#926-32211; RRID: AB_621843
Goat anti-Mouse IRDye 800CW	LI-COR	Cat#926-32210; RRID: AB_621842
Bacterial and virus strains		
Hepatitis A virus HM175/18f	BEI Resources	Cat#NR-137
Encephalomyocarditis virus	BEI Resources	Cat#NR-46441
HAV-nLuc	Lab of Stanley Lemon (Rivera-Serrano et al., 2019)	N/A
Enterovirus 71 (MP4)	Provided by Jan Carette; described in Huang et al., 2012	N/A
Rhinovirus A2	Provided by Jan Carette; original source ATCC	VR-482
HCV JFH1	Provided by Jan Carette; described in Wakita et al., 2005	N/A
HEV infectious clone (genotype 3)	NIH/NIAID (Shukla et al., 2012)	N/A
Chemicals, peptides, and recombinant proteins		
RG7834	MedKoo Biosciences	Cat#563793; CAS#2072057-17-9 (S-isomer)
Critical commercial assays		
KAPA HiFi HotStart ReadyMixPCR Kit	Kapa Biosciences	KK2602
MEGAscript T7 Transcription Kit	Invitrogen	AM1333
Lipofectamine 3000	Invitrogen	L3000008
QuickExtract	Lucigen	QE09050

REAGENT OR RESOURCE	SOURCE	IDENTIFIER
Power SYBR Cells-to-CT kit	Invitrogen	44-029-55
QIAGEN Viral RNA Mini kit	QIAGEN	52904
Nano-Glo assay buffer	Promega	N1110
NEBuilder HiFi DNA Assembly Master Mix	New England BioLabs	E2621L
TransIT LT1 Transfection Reagent	Mirus Bio	MIR2300
QIAamp DNA Blood Maxi Kit	QIAGEN	51192
Protein G magnetic Dynabeads	Thermo Scientific	10-003-D
SF Cell Line 4D-Nucleofector™ X Kit L	Lonza	V4XC-2012
Luciferase Assay System	Promega	E1500
Poly(A) Tail-Length Assay Kit	Thermo Fisher Scientific	764551KT
Direct-zol RNA Microprep Kit	Zymo Research	R2050
NorthernMax Kit	Thermo Fisher Scientific	AM1940
DIG Northern Starter Kit	Sigma Aldrich	12039672910
Cell Titer Glo	Promega	Cat#G7570
Experimental models: cell lines		
HEK293FT	Thermo Scientific	Cat#R70007
U2OS	Lab of Ron Kopito (Walczak et al., 2019)	N/A
Huh7.5.1	Lab of Frank Chisari (Zhong et al., 2005)	N/A
HepG2-NTCP-K7	Lab of Ulrike Protzer (Ko et al., 2018)	N/A
HepAD38	Lab of Christoph Seeger (Ladner et al., 1997)	N/A
Huh7.5.1 HAVCR1 KO	This study	N/A
Huh7.5.1 SLC35A1 KO	This study	N/A
Huh7.5.1 PAPD5 KO, addback, and catalytic addback	This study	N/A
Huh7.5.1 PAPD7 KO	This study	N/A
Huh7.5.1 PAPD5/7 DKO	This study	N/A
Huh7.5.1 ZCCHC14 KO, and addback	This study	N/A
Huh7.5.1 UBA5 KO, addback, and catalytic addback	This study	N/A
Huh7.5.1 UFM1 KO, addback, Gly83 mutant, and ΔC3 conjugation mutant	This study	N/A
Huh7.5.1 UFSP2 KO	This study	N/A
Huh7.5.1 VPS4A KO	This study	N/A
Huh7.5.1 eIF4B ±	This study	N/A
Huh7.5.1 + WT RPL26-FLAG	This study	N/A
Huh7.5.1 + 5KR RPL26-FLAG	This study	N/A
Huh7.5.1 UFM1 KO + WT RPL26-FLAG	This study	N/A
Huh7.5.1 UFM1 KO + 5KR RPL26-FLAG	This study	N/A
Huh7.5.1 UFSP2 KO + WT RPL26-FLAG	This study	N/A

REAGENT OR RESOURCE	SOURCE	IDENTIFIER
Huh7.5.1 UFSP2 KO + 5KR RPL26-FLAG	This study	N/A
Oligonucleotides		
PCR primers, see Table S3	This study	N/A
gRNA oligos, see Table S3	This study	N/A
qPCR primers, see Table S3	This study	N/A
Recombinant DNA		
lentiCas9-Blast	Lab of Feng Zhang (Sanjana et al., 2014)	Addgene Plasmid #52962
human GeCKO v2 library	Lab of Feng Zhang (Sanjana et al., 2014)	Addgene Plasmid #1000000049
px458	Lab of Feng Zhang (Ran et al., 2013)	Addgene Plasmid #48138
UBA5 cDNA	Dharmacon	cDNA Accession: BC009737, Clone ID: 3879061
UFM1 cDNA	Dharmacon	cDNA Accession: BC005193, Clone ID: 3829206
RPL26 cDNA	OriGene	Cat#RC209922
ZCCHC14 cDNA	Dharmacon	cDNA Accession: BC101478, Clone ID: 8068984
pLenti CMV Puro DEST (w118-1)	Lab of Eric Campeau & Paul Kaufman (Campeau et al., 2009)	Addgene Plasmid #17452
PB-CMV-MCS-EF1α-Puro	Systems Biosciences	Cat#PB510B-1
pCI3 plasmids with WT or catalytic mutant cDNA sequences for PAPD5/PAPD7	Lab of Narry Kim (Lim et al., 2018)	N/A
pLuc-HAV/18f Replicon	Lab of Stanley Lemon (González-López et al., 2018)	N/A
pLuc-HAV/18f-3D^{pol} GDD→GAA (replication-defective mutant) Replicon	Lab of Stanley Lemon (González-López et al., 2018)	N/A
pCRBlunt II-TOPO vector	Invitrogen	Cat#K2800-20
Software and algorithms		
MaGeCK analysis (gene enrichment)	Li et al., 2014	https://sourceforge.net/p/mageck/wiki/Home/
Gorilla (Gene Ontology)	Eden et al., 2009	http://cbl-gorilla.cs.technion.ac.il
RIGER weighted sum algorithm (gene enrichment)	Luo et al., 2008	https://www.broadinstitute.org/rnai_analysis
Prism 8	GraphPad Software	https://www.graphpad.com/scientific-software/prism/
R 3.6.0	R	https://www.r-project.org
CFX Maestro Software	Bio-Rad	Cat #12004110
Deposited data		
Raw sequencing data for CRISPR KO screens	EMBL-EBI ArrayExpress	E-MTAB-8646